Accepted Manuscript

Journal of the Geological Society

Geochronology and geochemistry of the Tabaquito batholith (Frontal Cordillera, Argentina): geodynamic implications and temporal correlations in the SW Gondwana margin

Juan A. Moreno, Juan A. Dahlquist, Matías M. Morales Cámera, Pablo H. Alasino, Mariano A. Larrovere, Miguel A.S. Basei, Carmen Galindo, Priscila S. Zandomeni & Sebastian Rocher

DOI: https://doi.org/10.1144/jgs2019-062

Received 3 April 2019
Revised 21 November 2019
Accepted 25 November 2019

Supplementary material at https://doi.org/10.6084/m9.figshare.c.4763993

To cite this article, please follow the guidance at http://www.geolsoc.org.uk/onlinefirst#cit_journal

Geochronology and geochemistry of the Tabaquito batholith (Frontal Cordillera, Argentina): geodynamic implications and temporal correlations in the SW Gondwana margin

Juan A. Moreno[a*], Juan A. Dahlquist[a], Matías M. Morales Cámera[a], Pablo H. Alasino[b,c], Mariano A. Larrovere[b,c], Miguel A.S. Basei[d], Carmen Galindo[e], Priscila S. Zandomeni[a], Sebastian Rocher[b,c]

[a]Centro de Investigaciones en Ciencias de la Tierra (CICTERRA), Consejo Nacional de Investigaciones Científicas y Técnicas. Facultad de Ciencias Exactas, Físicas y Naturales, Universidad Nacional de Córdoba, Av. Vélez Sarsfield 1611, Edificio de CICTERRA, X5016CGA, Córdoba, Argentina

[b]Centro Regional de Investigaciones Científicas y Transferencia Tecnológica de La Rioja (Prov. de La Rioja-UNLaR-SEGEMAR-UNCa-CONICET), Entre Ríos y Mendoza s/n, Anillaco 5301, Argentina

[c]Instituto de Geología y Recursos Naturales, Centro de Investigación e Innovación Tecnológica, Universidad Nacional de La Rioja (INGeReN-CENIIT-UNLaR), Av. Gob. Vernet y Apóstol Felipe, 5300 La Rioja, Argentina

[d]Instituto de Geociências da Universidade de São Paulo, RAU do Lago, 562, São Paulo, SP 05508-080, Brazil

[e]Departamento de Mineralogía y Petrología, Facultad de Ciencias Geológicas. Universidad Complutense-Instituto de Geociencias (IGEO, CSIC), 28040 Madrid, Spain

*Corresponding author: Juan A. Moreno

e-mail: jmoreno_2@ugr.es, jumoreno1983@gmail.com

Telephone: +54 0351 - 5353800

Abstract

The Tabaquito batholith (Frontal Cordillera, western Argentina), is mainly composed of shallowly emplaced granodiorite to minor monzogranite with abundant mafic microgranular enclaves. New SHRIMP U–Pb zircon ages of ~337 Ma (biotite granodiorite) and ~284 Ma (mafic dyke) along with previously published geochronological data suggest a long-lived magmatic system formed through at least two magmatic pulses at ~337 Ma and ~322 Ma with later superposition of Permian magmatism. The Tabaquito granitoids are metaluminous, calc-alkalic and magnesian with I-type affinity. Elevated Th/Nb, Y/Nb and La/Nb ratios along with negative Nb-Ta and positive Pb anomalies are consistent with a continental arc setting. Hf, Nd and Sr isotopic composition of the Tabaquito granitoids suggests their source could result from mixing of an old felsic crustal component and a juvenile mafic to intermediate component.

New geochronological and geochemical data together with published data reveal a continuous arc setting from the Carboniferous to the Permian in Argentina, and important magmatic compositional variations through time and space controlled by episodic fluctuations in the subduction angle of the oceanic plate. Reported and compiled data allow us to infer the continuity of the Carboniferous magmatic arc along the west margin of Gondwana.

Keywords

Frontal Cordillera, pre-Andean magmatism, calc-alkaline I-type granitoids, Carboniferous and Permian, shallow emplacement, incremental growth, subduction angle

The proto-Andean margin of SW Gondwana has constituted an accretional margin from at least the earliest Ordovician until the present (Cawood 2005). It experienced several magmatic events in the Palaeozoic, which are well preserved and exposed in the Sierras Pampeanas of NW Argentina (26º–32ºS latitude) (Fig. 1). Available geochronological data have allowed the identification of four main magmatic events (e.g. Pankhurst & Rapela 1998; Siegesmund *et al.* 2004; Dahlquist *et al.* 2008, 2013, 2016; 2018a; von Gosen *et al.* 2014; Coira *et al.* 2016; Casquet *et al.* 2018): 1) Pampean magmatism, 535–515 Ma; 2) Famatinian magmatism, 484–463 Ma; 3) Achalian magmatism, 393–366 Ma; and 4) Early Gondwana magmatism, 357–322 Ma. Recently, Dahlquist *et al.* (2018a) have concluded that the Achalian and Early Gondwana magmatism define a long-lasting magmatic event (ranging from 379 to 322 Ma) on the pre-Andean margin of SW Gondwana between 28º– 33º S latitude, although important whole-rock and isotopic compositional variations occurred through time and space.

In the last twenty years, understanding of the petrogenesis of Pampean and Famatinian magmatism has considerably improved (e.g. Pankhurst & Rapela 1998; Lira *et al.* 1997; von Gosen *et al.* 2014; Alasino *et al.* 2014; Ducea *et al.* 2015; Larrovere et *al.* 2015; Otamendi *et al.* 2017; Casquet *et al.* 2018), although late Devonian and Carboniferous magmatism remain by contrast comparatively poorly understood (e.g. Dahlquist *et al.* 2014, 2016, 2018a).

The late Devonian – early Carboniferous geodynamical setting of the pre-Andean margin of Gondwana is particularly controversial (Alasino *et al.* 2012; Dahlquist *et al.* 2018a and references therein). Inasmuch as some authors argue for the lack of clear evidence for the existence of a pre-Andean magmatic arc before the late Carboniferous (~320 Ma; Dormeier & Torsvik, 2014). In agreement with this, several authors indicate

that this was a passive margin in the Devonian (~420–360 Ma), based on the record of detrital zircon ages in early Carboniferous basins (e.g. Bahlburg *et al.* 2009; Hervé *et al.* 2013, 2016). Others (e.g. Willner *et al.* 2011 and references therein) advocate for a subduction margin followed by middle–late Devonian (~390 Ma) collision between Gondwana and a hypothetical terrane (Chilenia), with subsequent emplacement of early Carboniferous (~340 Ma) post-collisional granites in the Frontal Cordillera that remain unproven. By contrast, recent works (Alasino *et al.* 2012; Dahlquist *et al.* 2018a) postulate continuous magmatism during late Devonian and early Carboniferous characterised by marked compositional changes in space and time, likely as a consequence of fluctuations in the angle of subduction of the oceanic plate (geodynamic switching model). This resulted in coeval generation of subduction-related (calc-alkaline I-type) and retro-arc (A-type) Carboniferous magmatism (Fig. 1) (Alasino *et al.* 2012; Dahlquist *et al.* 2015) after a period of predominantly peraluminous A-type magmatism during the late Devonian (Dahlquist *et al.* 2018a).

The number of works on the Carboniferous magmatism have significantly increased in the last eight years but they mainly focus on the intracontinental A-type magmatism from eastern Sierras Pampeanas (Grosse *et al.* 2009; Dahlquist *et al.* 2010, 2013, 2016, 2018a; Alasino *et al.* 2012, 2017; Morales Cámera *et al.* 2017, 2018), whereas the calc-alkaline magmatism that crops out in the Frontal Cordillera and Western Sierras Pampeanas remains poorly studied (Llambías & Sato 1995; Dahlquist *et al.* 2015, 2018a, 2018b). Therefore, systematic studies that characterise and discuss the petrogenesis of the calc-alkaline plutons from Frontal Cordillera are needed to better understand the Carboniferous subduction-related magmatism.

Although, the Andean subduction is one of the Earth's main plate boundaries, a complete comprehensive geodynamic model for the palaeo-South American central

western margin in Argentina does not exist. In agreement with del Rey *et al.* (2016), the Chilean and Argentine Frontal Andes batholiths, together with the Coastal Batholith, represent most of the pre-Andean orogenic cycle plutonism (Andean orogenic cycle bearing during the early Jurassic) and its study is relevant to establish comparisons between the pre-Andean and the Andean magmatism. In the Frontal Cordillera, Carboniferous calc-alkaline magmatism was recently described in a broad-brush approach by Dahlquist *et al*. (2018a), but how the Carboniferous magmatism occurred along this margin previous to the Andean orogenic cycle as well as details about its petrology and geochemistry still remain unclear.

The present work aims to perform an integrated mineralogical and geochemical characterisation of the Tabaquito batholith, located in the Frontal Cordillera (western Argentina), which constitutes a large outcrop (896 km^2) of the early Carboniferous calc-alkaline magmatism (Llambías & Sato, 1995; Dahlquist *et al.* 2018a). This magmatism remains poorly studied and is normally represented by small granitic plutons, which contrast with the large dimensions of the Tabaquito batholith. Such dimensions make the batholith an exceptional example for studying the generation of calc-alkaline magmas in the SW margin of Gondwana. Furthermore, future detailed geochronological and geochemical studies complementing those initiated here will help understand the formation of arc-related batholiths.

We present new U–Pb zircon ages along with new whole-rock compositions (major and trace elements), Nd and Sr isotopes, mineral chemistry of the major mineral assemblage, and P-T estimations. These data are integrated with those reported by Llambías & Sato (1995) and Dahlquist *et al.* (2018a) as a first step to understand the petrogenesis of the batholith. The results are compared with available chemical data of other Carboniferous subduction-related plutons from Argentina and Chile to give a

wider view of the subduction-related granitic magmatism at the pre-Andean margin of SW Gondwana during the Carboniferous.

Geological setting: The Frontal Cordillera and Tabaquito batholith

Frontal Cordillera

The Frontal Cordillera is a morphostructural province involved in the Andean orogeny, located to the west of Precordillera and stretched between 27º S and 34º45' S latitude in Argentina, as well as between 27º S and 31º S latitude in Chile (Caminos, 1979; Maksaev *et al.* 2014; Sato *et al.* 2015) (Fig. 1).

The stratigraphic section of the Frontal Cordillera can be divided into three major representative units (Sato *et al.* 2015 and references therein):

1) Pre-Carboniferous basement units that consist of Mesoproterozoic orthogneisses, Ediacaran to Cambrian rocks sequences affected by Devonian high-pressure metamorphism, and Ordovician and Devonian sedimentary rocks (Chinguillos and Ciénaga del Medio groups) with intrusions of Devonian plutonic rocks.

2) Carboniferous to Triassic sedimentary and igneous sequences. Among the most notable are the Cerro Agua Negra formation, the Colangüil batholith, and volcanic and plutonic rocks of the Choiyoi group. The youngest rocks of the later are associated to an extensional environment.

3) Rock sequences assigned to the Andean orogeny that mainly consist of early Jurassic to Neogene sedimentary and volcanic rocks.

The Carboniferous magmatism of the Frontal Cordillera and Western Sierras Pampeanas (Fig. 1) has long been considered part of a probable Carboniferous magmatic arc (e.g. Llambías & Sato, 1995; Alasino *et al.* 2012, Dahlquist *et al.* 2015, 2018a). This magmatism, in the area between 28ºS latitude and 30ºS latitude, is

represented by isolated granitic bodies that occur as scattered plutons of variable size throughout the region (Fig. 1). These plutons are poorly studied although new geochronological data together with a brief geochemical characterisation of most of the plutons have been recently reported in a regional or broad-brush approach work (Dahlquist *et al*. 2018a). The plutons that belong to this arc-related magmatism are the following:

1) Potrerillos pluton (353 ± 2 Ma; Dahlquist *et al.* 2018a). An elliptical intrusive body of ca. 78 km^2 (south of Sierra del Toro Negro; Fig. 1) mainly formed of an amphibole-biotite quartz-diorite with mafic microgranular enclaves and a porphyritic biotite granodiorite.

2) Las Tunas pluton (324 ± 6 Ma by K-Ar method; Caminos, 1972) is a small granitic pluton located in the Frontal Cordillera to the west of Sierra del Toro Negro (Fig. 1).

3) Río Bonete stock (342 ± 5 Ma; Dahlquist *et al*. 2018a). An intrusive body of approximately 2 km^2 in the northeastern part of the Precordillera and south of Sierra del Toro Negro (Fig. 1). It consists of two facies one represented by a dark equigranular medium-grained gabbro, and another by a coarse-grained porphyritic monzonite.

4) Veladero stock (342 ± 2 Ma; Dahlquist *et al.* 2018a) that is an intrusive body approximately of 9 km^2 in the eastern flank of the Precordillera and the western part of the Western Sierras Pampeanas (Sierra de Umango) (Fig. 1). This granitic stock is made of quartz-poor monzogranite, quartz-monzonite, monzodiorite, and syenogranite.

5) Guandacolinos pluton (357± 2 Ma; Dahlquist *et al.* 2018a). It crops out over an area of 24 km^2 in the western flank of the Sierra de Umango (Fig. 1) and is made of monzogranite to granodiorite with biotite and scarce amphibole.

6) Tabaquito batholith (322 ± 5 Ma; Dahlquist *et al.* 2018a) located in the Frontal Cordillera (Fig. 1) and described below. This batholith, which is the subject of this study, is located in the Frontal Cordillera north of the Colangüil batholith (San Juan province; Fig. 1). The term "Colangüil batholith" was first coined by Quartino & Zardini (1967) in reference to the various plutonic acid rocks that crop out between the Santa Rosa and Agua Negra creeks, whereby the so-called "Tabaquito pluton" was considered part of the batholith (Llambías & Sato, 1995). According to previous studies (Llambías & Sato, 1990, 1995; Sato *et al.* 2015) the lithostratigraphy of the Colangüil region consists of an upper Carboniferous granodiorite to monzogranite pluton ("Tabaquito pluton", 322 ± 5 Ma; Dahlquist *et al.* 2018a) and several Permian granodioritic and granitic plutons (252–279 Ma; Sato *et al.* 2015). Consequently, although the "Tabaquito pluton" has been firstly considered part of the Colangüil batholith its Carboniferous age precludes this possibility. The country rocks of the various igneous bodies are metasedimentary rocks of the Chinguillos and Cerro Agua Negra Formations that consist of marine siliciclastic sequences of Devonian and Carboniferous to Permian age, respectively (Sato *et al.* 2015).

Field characteristics of the Tabaquito batholith

The Tabaquito igneous body crops out over an area of about 896 km^2 to the north of the Colangüil batholith (Fig. 2). We propose to use the term Tabaquito batholith instead of pluton because of its significant dimensions (>> 200 km^2; see batholith definition in Chapter 14 of Pitcher, 1993) and the difference in age between samples found in this study as discussed in the "geochronological implications" section. The batholith is mostly covered by Quaternary sedimentary deposits and contacts between rocks are hard to find in this area due to strong erosion under high mountain weather conditions, since most of the batholith crops out above 3500 masl (metres above sea

level). Thus, a detailed geochronological study is essential to establish the sequence of emplacement.

Our field studies confirm that the batholith is mainly formed of equigranular medium-grained grey granodiorites (Fig. 3A) that can be locally porphyritic with 70 vol.% phenocrysts (0.6–5 mm) and 30 vol.% matrix (<0.5 mm), although minor monzogranite compositions have also been reported by Llambías & Sato (1995). Field relations between equigranular and porphyritic varieties could not be observed. Their main mineral assemblage is represented by plagioclase + quartz + alkali feldspar + biotite + opaque minerals ± amphibole (see detailed petrography in supplementary file S1). They contain abundant biotite and amphibole-bearing mafic microgranular enclaves of centimetre- to decimetre-scale (Fig. 3A). Although the biotite rich and amphibole poor enclaves are the most common (Llambías & Sato, 1995), there also exists scarce biotite-amphibole rich enclaves with the common occurrence of amphibole clots, which are described here for the first time (see detailed petrography in supplementary file S1).

The batholith intrudes metasedimentary rocks of the Chinguillos Formation of Devonian age (Figs. 2 and 3B, C) and it is intruded to the south by the El Fierro pluton that belongs to the Los Puentes granite, with biotite/whole-rock Rb–Sr and LA-ICP-MS U–Pb ages that vary between 257 ± 1 and 253 ± 2 Ma (Llambías & Sato, 1995; Sato *et al.* 2015). However, our fieldwork in the southern part of the batholith reveals the existence of metre-size small outcrops of a fine-grained leucogranite (Fig. 3D) that consists of quartz (38 vol.%), alkali feldspar (33 vol.%), plagioclase (27 vol.%) and biotite (2 vol.%), and outcrops of a coarse-grained porphyritic granite (Figs. 2 and 3E) made of alkali feldspar (35–38 vol.%), quartz (34–38 vol.%), plagioclase (24–27 vol.%), biotite (2–4 vol.%) and muscovite (<1.5 vol.%), which have not been studied

yet. The coarse-grained porphyritic granite is in turn cut by aplitic dykes (Fig. 3F). Elsewhere, the eastern and western limits are truncated by Neogene Andean tectonic structures as reported by Sato *et al.* (2015). The batholith is also intruded by "radial" dyke swarms of mainly andesitic composition with subordinate dacitic to rhyolitic compositions, which in turn, are crosscut by N–S mainly rhyolitic dykes probably related to the Permian magmatism of the Choiyoi group (Llambías & Sato, 1995). The middle-upper Mississipian age of the Tabaquito batholith was first estimated by Rb–Sr isochrons (326 to 329 Ma; Llambías & Sato, 1995) and subsequently corroborated by LA-MC-ICP-MS U–Pb zircon dating (322 ± 5 Ma; Dahlquist *et al.* 2018a).

Samples and methods

For this study, we collected nine samples from the Tabaquito batholith (five from the host granodiorite, one mafic enclave, one mafic dyke and two felsic dykes). Mineral compositions were determined in three samples (two host equigranular amphibole-bearing granodiorites and one mafic enclave). Whole-rock major and trace element compositions were determined for the whole set of samples, and three samples (TAB-11, TAB-24 and TAB-32) has been also analysed for Nd and Sr isotopes. For U–Pb zircon dating, zircon grains were separated from one biotite-bearing sample from the south of the batholith (TAB-24) and one mafic dyke (TAB-40) from the north. Detailed information about analytical procedures of the mentioned methods are found in supplementary material (Text S1 and Table S1). This study also integrates previous published data (geochemical, geochronological and isotope data) from Llambías & Sato (1995) and Dahlquist *et al.* (2018a).

Mineral chemistry

Feldspars

Plagioclase in the granodiorite is essentially andesine ($An_{30–49}$; Fig. 4A) showing compositional zoning with cores richer in calcium ($An_{42–49}$) than rims ($An_{30–37}$) (Table 1). The composition of alkali feldspar is less variable and ranges from Or_{89} to Or_{96} (Fig.4A; Table S2).

Plagioclase from the mafic enclaves is also andesine (Fig.4A) with compositions similar to those of the granodiorite. Phenocrysts are characterised by compositions that vary between An_{38} and An_{48} with a poikilitic outer rim of oligoclase composition ($An_{21–25}$) (Table S2). They also show complex zoning with patches of oligoclase composition (An_{25}). Matrix plagioclase have cores of andesine composition ($An_{42–46}$) and rims of oligoclase composition ($An_{21–31}$) (Table S2).

Biotite

Trioctahedral mica from both the granodiorite and the enclaves is annite (Fig.4B) with very uniform $Mg/(Mg+Fe^{2+})$ of 0.46–0.52 (Table S2). Li contents calculated by the method described by Tischendorf *et al.* (2004) are low (0.05–0.06 apfu) (Table 2). F and Cl contents are very low, being F slightly higher than Cl with values of 0.04–0.15 apfu and 0.02–0.05 apfu respectively (Table S2).

In the MgO-FeO-Al_2O_3 diagram from Abdel-Rahman (1994) (Fig.4C), all analyses plot in the field of calc-alkaline granitoids, which is in accordance with the expected I-type affinity of these magmas.

Amphibole

Amphibole in the granodiorite is magnesio-hornblende (Fig.4D) and in the mafic clots show alteration to actinolite. Analysed amphibole from the mafic clots and single

crystals has Mg/(Mg+Fe^{2+}) of 0.57–0.74, low Ti (0.01–0.18 apfu) and very low F and Cl contents (0–0.15 apfu and 0.01–0.05 apfu respectively). Note that the single crystals have higher Ti (0.09–0.18 apfu) and lower Mg/(Mg+Fe^{2+}) (0.57–0.60) than amphibole from the mafic clots. It is noteworthy that analyses from sample TAB-11, collected in the northern part of the batholith, have higher Mg/(Mg+Fe^{2+}) than those from sample TAB-34 (Fig. 4D and Table S2) collected in the southern sector.

Amphibole from the quartz-dioritic enclaves is also magnesio-hornblende (Fig. 4D) although it presents higher alteration to actinolite in the amphibole clots. Amphiboles from the clots are chemically similar to those of the clots in the granodiorite, with Mg/(Mg+Fe^{2+}) of 0.62–0.72, low Ti (0.01–0.10 apfu) and very low F and Cl contents (≤0.07 apfu and 0.01–0.02 apfu respectively). Amphibole from the matrix and those included in plagioclase phenocrysts are similar in composition with Mg/(Mg+Fe^{2+}) of 0.57–0.67, Ti (0.07–0.18 apfu), F (0–0.15 apfu) and Cl (0.01–0.03 apfu) (Table S2).

Epidote

Primary epidote from sample TAB-34 (granodiorite) has pistacite content (Ps (%) = Fe^{+3}/(Fe^{+3}+Al) x 100) of 23–28 and very low TiO_2 content (<0.1 wt.%) (Table S2), which are typical values of magmatic epidote (Evans & Vance, 1987; Vynhal *et al.* 1991; Dahlquist 2001).

U–Pb zircon dating

In this section we present new U–Pb zircon data for samples TAB-24 and TAB-40 (Table 1).

TAB-24

More than 100 zircon grains from sample TAB-24 (porphyritic biotite-bearing granodiorite from the southern sector of the batholith) were studied by

cathodoluminescence, from which 12 grains were analysed by SHRIMP. The analysed zircons tend to have relatively elevated common lead. The studied zircons are mainly euhedral, prismatic with bipyramidal terminations (supplementary file S2), although scarce fragmented and rounded grains are also present. Under the cathodoluminescence microscope most zircons show well-developed oscillatory zoning (supplementary file S2) but sector zoning and homogeneous textures have been also recognised. The analyses were carried out mainly on rims or edge zones of selected grains to obtain the crystallisation age (Table 1). The whole set of analysed zircons yielded a $^{206}Pb/^{238}U$ age of 337 ± 2 Ma (n=12, MSWD = 0.022; Fig. 5A) that is the same as the $^{206}Pb/^{238}U$ age obtained when we use only the most concordant analyses (338 ± 2 Ma, discordance < 10%, n = 9, MSWD = 0.00069). Therefore, we consider the age of 337 ± 2 Ma as the crystallisation age of this sample, which is older than the "previous U–Pb age" of 322 ± 5 Ma reported by Dahlquist *et al.* (2018a) in the northern part of the batholith.

TAB-40

Thirty-two zircon grains from sample TAB-40 (a N-S mafic dyke from the north of the batholith) were studied by cathodoluminescence, from which 12 grains were analysed by SHRIMP (Table 1). The studied zircons are mostly rounded and fragmented grains with sector and oscillatory zoning (supplementary file S3). Homogeneous bright and dark zones are also common (supplementary file S3). Four U–Pb determinations made on four of the twelve analysed zircon grains yielded a $^{206}Pb/^{238}U$ age of 284 ± 4 Ma (MSWD = 0.067; Fig. 5B) that may represent the crystallisation age of the dyke. However, seven U–Pb concordant determinations done on seven zircons gave a $^{206}Pb/^{238}U$ age of 336 ± 3 Ma (MSWD = 0.0052; Fig. 5B) that overlaps with the crystallisation age of sample TAB-24.

Whole-rock chemistry

In this section we use new major and trace element data of granitoids and dykes (Table 2) along with data from Llambías & Sato (1995) to characterise the magmatism of the Tabaquito batholith.

Granodiorites and monzogranites that form the batholith are magnesian ($FeO_T/(MgO + FeO_T)$ by weight = 0.66–0.75), calc-alkalic (MALI = $Na_2O+K_2O–CaO$ by weight) = 2.65–5.2) and metaluminous to weakly peraluminous (Alumina saturation index, ASI = 1.00–1.12) (Fig. 6A-C), with 65.5–70.5 wt.% SiO_2, 14.5–15.9 wt.% Al_2O_3, 0.39–0.69 wt.% TiO_2, 2.69–4.46 wt.% FeO and 1.11–2.26 wt.% MgO (Table 2). The studied quartz–dioritic enclave is strongly magnesian (Fe–number = 0.56), alkali-calcic (MALI = 1.12) and metaluminous (ASI = 0.86) (Fig. 6A-C). Both the Tabaquito granitoids and the enclave are potassium rich rocks (3.08–4.32 wt.% K_2O; Fig. 6D).

The three dykes samples plot in the fields of basaltic trachyandesite (TAB-40), dacite (TAB-41) and rhyolite (TAB-23) of the TAS diagram (Fig. 6E). Furthermore, as sample TAB-40 has $Na_2O - 2 \leq K_2O$, it is additionally classified as a shoshonite. They are high-K, magnesian to ferroan ($FeO_T/(MgO + FeO_T)$ by weight = 0.67–0.94), calc-alcalic to alkali-calcic (MALI = $Na_2O+K_2O–CaO$ by weight) = 0.93–8.58) and peraluminous (ASI = 1.03–1.18) (Fig. 6A-C).

In Harker diagrams, the Tabaquito granitoids show negative correlations between silica and FeO, MgO, TiO_2, Al_2O_3 and P_2O_5 (Fig. 1 in supplementary material), whereas Na_2O is nearly constant and CaO shows higher dispersion, although with a tendency to decrease as silica increases (Fig. 1 in supplementary material).

Chondrite-normalised REE patterns of the Tabaquito granitoids show a moderately negative slope (La_N/Lu_N = 6.74–10.14) with a small negative Eu anomaly (Eu/Eu* =

0.62–0.79), and they are nearly flat from Ho to Lu (Fig. 7A). The enclave shows a similar pattern (La_N/Lu_N = 4.18; Eu/Eu* = 0.68) but with lower La and higher MREE and HREE values (Fig. 7A). Both the host granodiorite and the enclave have similar REE contents to other arc-related Carboniferous plutons from Argentina although the Tabaquito granitoids are less enriched in LREE with respect to HREE (Fig. 7A). Silicate Earth normalised trace-element patterns are enriched in incompatible elements showing negative Ba, Nb-Ta, P and Ti anomalies along with a positive Pb anomaly (Fig. 7B). Note the negative Th anomaly of the enclave that contrasts with the relatively high Th values of the granodiorites (Fig. 7B). The studied samples plot within the compositional range of the Argentine arc-related Carboniferous magmatism (Fig. 7B) and strongly contrast with the REE pattern and spider/multielement diagram reported for the Carboniferous A-type magmatism (e.g. Dahlquist *et al.* 2010, 2018a).

REE and trace elements compositions of the dykes are similar to those described for the Tabaquito granitoids although the dacite dyke (TAB-41) has slightly lower values of REE (Fig. 7).

Nd and Sr Isotopes

Sr and Nd isotope compositions of the studied samples (TAB-11, TAB-24 and TAB-32) and Sr isotope compositions taken from Llambías & Sato (1995) are listed in Table 2. Initial radiogenic isotope ratios were calculated at crystallisation ages (322 Ma and 337 Ma; Dahlquist *et al.* 2018a and this study). Nd model ages (T_{DM}) were calculated according to the expression derived by DePaolo (1981). The $^{147}Sm/^{144}Nd$ ratios in the analysed samples are below the threshold value of 0.165, above which calculated model ages tend to be unreliable (see discussion in Stern, 2002).

The studied samples present εNd_i values that range between –1.61 and –2.38, along with Nd model ages that vary between 1091 and 1113 Ma. The Sr parameters of the studied samples (Sr/Sr_i = 0.7053 to 0.7056) are in the range of those calculated from the Llambías & Sato (1995) data (Sr/Sr_i = 0.7039–0.7071), except one sample with a clearly higher value (Sr/Sr_i = 0.7095). Note that isotope values of the amphibole-bearing granododiorite (TAB-11) and biotite-bearing porphyritic granodiorite (TAB-24) as well as those of the enclave (TAB-32) are nearly the same although the biotite-bearing porphyritic granodiorite has slightly lower εNd_i (Table 2).

P-T conditions

Crystallisation conditions for rocks of the Tabaquito batholith have been determined using amphibole-only and amphibole-plagioclase thermobarometric expressions (Schmidt 1992; Holland & Blundy 1994; Ridolfi & Renzulli 2012; Molina *et al.* 2015; Mutch *et al.* 2016; Putirka 2016). A summary of the calculated amphibole-only and amphibole-plagioclase P-T conditions for samples TAB-11 (north of the batholith), TAB-32 and TAB-34 (south of the batholith) is presented in Table 3. Temperatures calculated with the diverse amphibole-only calibrations are similar (range: 705–810 ºC; Table 3), being virtually the same when considering the error of each calibration.

Al–in–amphibole pressure estimates for amphibole from the amphibole clots and single crystals in granodiorites (TAB-11 and TAB-34) vary between 1.4–3.1 kbar for the different calibrations (Table 3). The pressure calculated with the plagioclase–amphibole barometer of Molina *et al.* (2015) gave 1.7 ± 0.6 kbar at 750 ºC (Table 3). Therefore, the pressure estimates for rim compositions of the single crystals and for amphibole from the clots (<2.5 kbar; Table 3) indicate a shallow emplacement of these magmas.

Temperatures for amphibole of the clots calculated with the amphibole-only thermometers range from 720 ºC to 785 ºC (Table 3). In the case of single crystals, temperatures vary between 738 ºC and 810 ºC. Temperatures calculated at 2 kbar with the amphibole-plagioclase thermometer (Holland & Blundy 1994) for the individual crystals are 754 ± 30 ºC (Ed–Q–Tr–Ab expression) and 767 ± 20 ºC (Ed–Ab–Rich–An expression) (Table 3), which match those of the amphibole-only thermometers. On the other hand, in the case of amphibole from the clots the Ed–Q–Tr–Ab thermometer gives temperatures excessively low, being sometimes more than 150 ºC lower than those obtained with the Ed–Ab–Rich–An thermometer that are closer to those of the amphibole–only thermometer. It could be a consequence that these clots were not in equilibrium with quartz, since for these analyses unrealistic pressures have been obtained with the barometer of Molina *et al.* (2015), which works better in mineral assemblages in equilibrium with quartz and/or clinopyroxene. Consequently, we have only considered the Ed–Ab–Rich–An thermometer that gives temperatures of 692–776 ºC for plagioclase compositions of $An_{30–37}$ and 720–825 ºC for $An_{42–49}$ (Table 3).

The mafic enclave (sample TAB-32) has pressures of 0.8–3.3 kbar calculated with the different barometers (Table 3). Temperatures calculated with the amphibole-only thermometers are similar for amphiboles from the matrix, the clots and those included in plagioclase phenocrysts (range: 705–810 ºC), which are also similar to those obtained for amphiboles from the host granodiorite. Temperatures calculated with the amphibole–plagioclase thermometers are 641± 27 ºC (Ed–Q–Tr–Ab) and 666 ± 32 ºC (Ed–Ab–Rich–An) for matrix amphibole and plagioclase composition of $An_{21–46}$, and 742 ± 15 ºC (Ed–Ab–Rich–An) for amphibole from the clots and plagioclase of $An_{42–49}$. In the case of amphibole included in plagioclase phenocrysts the pairs have been made only with the plagioclase that host the inclusions and there are two possibilities: those

that behave like the single crystals of the host granodiorite, with similar temperatures for the two calibrations (762 ± 14 ºC and 756 ± 10 ºC, respectively); and those that behave like amphibole from the clots (726 ± 11 ºC; Ed–Ab–Rich–An). Therefore, the obtained amphibole temperatures and pressures, excepting those from the matrix that are lower, are in the range of those from the host granodiorite.

Discussion

Petrogenesis of the Tabaquito batholith

Chemical and mineralogical characterisation of the granitoids

Major and trace element compositions along with the mineral assemblages of the Tabaquito granitoids correspond to high-K magmas of I-type affinity formed in a subduction environment. The studied granites are calc-alkalic and magnesian (Fig. 6A, B), mostly ploting in the sub-alkaline field in the TAS diagram (Fig. 6E), and their mafic assemblage is characterised by biotite, hornblende and magnetite, indicating an I-type affinity. These rocks are enriched in incompatible elements and present negative Nb-Ta and positive Pb anomalies, which are distinctive of common subduction-related sources. Relationships of Th/Nb, Y/Nb and La/Nb ratios, sensitive to magma sources (e.g. Moreno *et al.* 2014, 2016), also point to an evident subduction-related source for the Tabaquito granites (Fig. 8), with compositions similar to those of rocks generated in continental arcs and shoshonitic suites (Fig. 8A). Consistently, biotite composition indicates a calc-alkaline source for these magmas (Fig. 4C), whereas Ti contents versus Mg, Na, K and Al contents of amphibole suggest a subalkaline affinity (Fig. 2 in supplementary material; Molina *et al.* 2009).

Chemical and isotopic constraints of the source

These granites have distinctive high-K content (see description in the "whole-rock chemistry" and "chemical and mineralogical characterisation of the granitoids" sections). The origin of high-K calc-alkaline I-type granites is a controversial issue mainly due to the large range in isotopic compositions, which contributes to the discussion of whether mantle-derived mafic magmas contribute with material or only as a heat source (e.g. Clemens & Stevens 2012; Gao *et al.* 2016). Recent zircon Hf-isotope data of an equigranular amphibole-bearing granodiorite from the north of the Tabaquito batholith reported by Dahlquist *et al.* (2018a) (εHf range –2.0 to +4.5; sample TAB-11) suggest a mainly juvenile (mantle-like) source with certain involvement of an older crustal component. This is supported by the slightly negative εNd_i values of –1.6, −1.8 and −2.4 obtained in this study, and by the available Sr isotope data that present Sr/Sr_i mostly ranging between 0.7039 and 0.7071. Although further data are needed, the current isotopic data point to a mainly juvenile source with the involvement of older crustal material. The Nd model ages calculated here (~1.1 Ga) are similar to the average Hf model age (~1.2 Ga) reported by Dahlquist *et al.* (2018a), which might suggest partial melting of a late Mesoproterozoic source. However, this age may likely be an artefact that results from the mixing of a juvenile crustal or mantle end-member and an older crustal end-member, which is consistent with the isotopic parameters discussed previously. In relation to this, Dahlquist *et al.* (2018a) have suggested the plausible existence of two contrasting, coeval (353 Ma) and not consanguineous parental magmas in the Potrerillos pluton (located to the northeast of the Tabaquito batholith; Fig. 1). One of them has intermediate composition (55–62 wt.% SiO_2) and a clear juvenile signature (εHf ranging between +0.37 and +12.6), whereas the other is essentially felsic (67–73 wt.% SiO_2) with a strong crustal signature (εHf of –34.5 to −2.2). Hypothetically, subsequent melting events could give rise to the parental magmas of the Tabaquito

batholith (66 wt.% SiO_2 and variable isotopic parameters) as a result of the variable mixing of two components comparable to these. This hypothesis would also explain the crustal value of the Nb/Ta and $(Th/Ta)_N$ ratios of the studied rocks (Table 2), since it might be inherited from the crustal felsic component.

Emplacement conditions

Amphibole-based thermobarometric estimates for the Tabaquito granodiorite and the quartz-diorite enclave yield temperatures that mostly cluster around 750 ºC and pressures that mainly vary between 1 and 3 kbar (Table 3), with rim compositions and those of amphiboles from the clots giving a pressure range of ca. 1–2.5 kbar. Therefore, amphibole crystallisation could have started at pressures around 3 kbar but the emplacement pressure of these magmas should likely be lower than 2.5 kbar, independently of geographic location within the batholith.

Considering that the Tabaquito batholith and the Veladero stock (~1.8 kbar and ~725 ºC) are representatives of the Carboniferous subduction-related magmatism (Dahlquist *et al*. 2018a and references therein), this magmatism represents shallow structural levels (<10 km deep) of the arc.

Geochronological implications

The Tabaquito batholith

A Carboniferous age of 326−329 Ma for the batholith was firstly established by Llambías & Sato (1995) based on Rb-Sr whole-rock and mineral data. This age was later corroborated by a U-Pb zircon age of 322 ± 5 Ma obtained by Dahlquist *et al.* (2018a) (Fig. 9A) on an amphibole-bearing granodiorite from the north of the batholith (sample TAB-11; Fig. 2). In order to check these ages, we have dated a porphyritic biotite-bearing granodiorite from the south of the batholith (sample TAB-24), which

yielded a Carboniferous U–Pb zircon age of 337 ± 2 Ma (Fig. 5A) that is significantly older than the age of the sample from the northern sector. Interestingly, the sample TAB-11 dated by Dahlquist et al. (2018a) presents a group of zircons (n = 6), integrated in the calculated crystallisation age (Fig. 9A), with ages ranging between 330 and 347 Ma (Fig. 9; see supplementary file 2 in Dahlquist et al., 2018a). This range of ages overlaps the ages determined for the biotite-bearing granodiorite from the south (TAB-24, Concordia age = 337 ± 2 Ma) and correlates the magmatism in both areas (north and south), suggesting that the crystallisation could start around 337 Ma and finish at 322 Ma. Furthermore, the existence of an inherited magmatic zircon age of 336 ± 3 Ma in the early Permian dyke (Fig. 5B) from the north, which is interpreted as magmatic zircons collected from previously crystallised early Carboniferous granites (see next section below), is consistent with this interpretation.

Consequently, zircons from TAB-11 with ages between 330 and 347 Ma may be considered antecrysts, that is, zircon crystals that crystallised from earlier magma pulses and are incorporated in later pulses (e.g. Miller *et al.* 2007 and references therein). The presence of antecrysts formed at earlier stages and deeper levels that are remobilised and carried to the emplacement level through new magma pulses has been incrementally reported by several authors (Miller *et al.* 2007; Barboni *et al.* 2013; Paterson *et al.* 2016; Alasino *et al.* 2017; Dahlquist *et al.* 2018b, 2019; Siégel et al., 2018; and references therein). Accordingly, Spencer *et al.* (2016) asserted that a single age should not be assumed as representative of a pluton without a detailed geochronological study, because magmatic systems are often characterised by protracted events.

Despite the apparent difference in age, samples from both the south and the north of the batholith are alike in terms of whole-rock chemistry, mineralogy and P-T

conditions as described in previous sections. This might suggest an incremental growth of the batholith via several magma pulses with a likely common source and plumbing system that are apparently emplaced under similar conditions. In the recent literature, incremental growth of plutons and batholiths worldwide involving long periods of time has been reported by several authors (e.g. Coleman *et al.* 2004; Glazner *et al.* 2004; Paterson *et al*. 2016; Alasino *et al.* 2017; Hines *et al.* 2018; Dahlquist *et al.* 2019), contributing to the extended debate about how magmatic systems are built.

It is important to mention that we have reported twelve U–Pb zircon SHRIMP analyses for TAB-24, while Dahlquist *et al.* (2108a) reported twenty U–Pb zircon LA-MC-ICP-MS analyses for TAB-11. Consequently, we suggest that new zircon analyses are required to verify if TAB-24 has a similar zircon population to that from TAB-11 or not.

The intrusive dykes

Llambías & Sato (1995) attributed the intrusion of N-S dykes described in the "geological setting" and "whole-rock chemistry" sections, to the extensive Permian magmatism of the Choiyoi group (Permian to early Triassic), although the crystallisation age remained unknown.

The first U–Pb zircon ages of 284 ± 4 Ma and 336 ± 3 Ma (Fig. 5B) obtained here for sample TAB-40 (one N-S mafic dyke from the north of the batholith) confirm a lower Permian age for this dyke and reveal a significant inheritance of Carboniferous zircons whose age matches the older age found in the Tabaquito granites (Figs. 5A and 9). Thus, this evidence indicates that the dykes were developed and intruded into the granite during the early Permian, collecting magmatic zircon previously crystallised in the early Carboniferous granites.

Temporal correlations along the SW margin of Gondwana

U-Pb zircon data of this study together with data from the literature allow us to review the Carboniferous magmatism and correlations along the proto-Pacific margin of Gondwana, which according to Cawood (2005) has constituted an accretionary margin from at least the earliest Ordovician until the present.

In a regional view, the Carboniferous ages of the Tabaquito granitoids (337 to 322 Ma) are slightly younger that those reported for the other calc-alkaline plutons from the Frontal Cordillera and Western Sierras Pampeanas of Argentina (357–342 Ma; Dahlquist *et al*. 2018a, 2018b), although within error the age of 337 Ma is roughly coeval to those of 342 Ma (Río Bonette and Veladero stocks; Dahlquist *et al*. 2018a, 2018b). The correlative I-type calc-alkaline volcanic and plutonic rocks from the Chilean Frontal Cordillera and the Coastal Batholith have ages ranging between 328 ± 3 Ma and 301 ± 2 Ma (Deckart *et al.* 2014; Maksaev *et al.* 2014; del Rey *et al*. 2016) that are in general younger than their Argentine counterparts (357–322 Ma) although with a few overlapping ages (Fig. 10). Although southern granitic outcrops of such Carboniferous magmatism have not been reported in Chile so far (Pankhurst *et al.* 2006), this magmatism may be correlated with calc-alkaline I-type hornblende granitoids from the eastern North Patagonian Massif with Rb-Sr and U-Pb ages varying between 330 and 320 Ma (Pankhurst *et al*. 2006). These ages match the crystallisation ages of the Tabaquito batholith. Strikingly, I-type calc-alkaline granitoids from Eastern Cordillera (Perú), probably formed in a continental arc (Fig. 9; Mišković *et al.* 2009), yielded similar ages to those of the Chilean arc magmatism (330–301 Ma with inheritance of ~350 Ma; Chew *et al*. 2007; Mišković *et al.* 2009) and match the ages of the Argentine arc magmas. Therefore, based on current geochronological data from the

granites of Perú, Chile and Argentina we postulate a palaeo-Pacific continental arc that was active at least between 357 and 301 Ma ago.

Carboniferous I-type calc-alkaline granitoids have also been reported from various crustal blocks of West Antarctica (Antarctic Peninsula, Thurston Island, Mary Byrd Land, North Victoria Land; e.g. Leat *et al.* 1993; Pankhurst *et al.* 1993, 1998; Millar *et al.* 2002; Korhonen *et al.* 2010; Yakimchuk *et al.* 2015; Riley *et al.* 2017). These granitoids have ages of 358–343 Ma in the Mary Byrd Land (Pankhurst *et al.* 1998; Korhonen *et al.* 2010; Yakimchuk *et al.* 2015), ca. 347 Ma in the North Victoria Land (Henjes-Kunst & Kreuzer 2003) and ca. 349 Ma in the Thurston Island (Riley *et al.* 2017). These ages are comparable to those of the arc magmatism of Argentina (357–322 Ma; Fig. 10) but slightly older than those reported for the Chilean calc-alkaline granitoids (328–301 Ma; Fig. 10). These ages also find correlatives in the 351–342 Ma I-type granitoids of the Tobin suite from western New Zealand (Tulloch *et al.* 2009). It is also noteworthy that scarce SHRIMP U-Pb zircon data from the Antarctic Peninsula reveal a ~330 Ma thermal event (Millar *et al.* 2002) that coincides with the ages of the South American magmatism discussed here.

Tulloch *et al.* (2009) indicated that I-type granites of ca. 350–340 Ma age (Tobin Suite in New Zealand) constitute the only magmatic event that can be recognised throughout the entire Gondwana margin from both fold belts of eastern Australia to New Zealand, Marie Byrd Land, and possibly North Victoria Land. Consequently, this magmatic event can be now extended to the Thurston Island (West Antarctica) and South America as was described above. Therefore, the age correlation between South America, Antarctica and New Zealand suggest that these regions could have been contiguous in the Carboniferous (Fig. 11), forming an accretionary margin, although

with distinctive features in the subduction process (i.e., normal subduction, flat subduction, etc.).

Geodynamic model for the 27ºS–34ºS latitude

Considering that Carboniferous calc-alkaline rocks from Chile and Argentine at this latitude formed part of the same continental arc, here we compare their chemical and isotopic data to assess the characteristics of the geodynamic setting and their relation with the generation and evolution of the arc magmatism at this latitude.

The Argentine Carboniferous granites are richer in K_2O than their Chilean equivalents (Fig. 7D), which translates into higher alkalis contents plotting in the alkaline field of the TAS diagram and higher MALI values (Fig. 7B and 7E). This potassium enrichment is consistent with a continental arc in which the Carboniferous granitoids from Argentina would be located further away from the trench than their Chilean counterparts (Fig. 12A) (see discussion in Chapman *et al.* 2017). In such a scenario the increase in K_2O would either result from increasing depth of melting (Marsh & Carmichael, 1974) or from a greater involvement of the older continental crust (Hildreth & Moorbath, 1988). The isotopic data indicate that a greater participation of the older continental crust does not seem to be the cause of the K_2O enrichment observed in the Argentine granitoids. Thus, published Hf- and O-isotope zircon data (εHf_i = –34.5 to +14.1 and $\delta^{18}O$ = 6.1 to 7.3‰; Deckart *et al.* 2014; Dahlquist *et al.* 2018a) and Nd and Sr whole-rock isotope data (εNd_i = –1.7 to –4.2 and Sr/Sr_i = 0.7057–0.7098; Parada *et al.* 1981, 1999; Nasi *et al.* 1985) along with those obtained here, suggest variable involvement of mantle and crustal components in their sources, albeit with a likely greater imprint of the juvenile end-member in the Carboniferous Argentine granitoids (εHf_i ranging between –34.5 and +14.1 with predominance of positive values; Dahlquist *et al.* 2018a).

As revealed in the "geological implications" section, the Argentine granitoids at this latitude are older (357–322 Ma) than the Chilean correlatives (328–307 Ma) with a few overlapping ages (Fig. 10). Migration of the magmatism to the west could have been caused by steepening of the subducting plate during slab roll-back (Figs. 12A and B). Such a geodynamic scenario fits well within the geodynamic switching model that explains the coeval production of Carboniferous I-type arc and A-type retro-arc granitoids (Alasino *et al.* 2012; Dahlquist *et al*. 2018a).

As was described in the "field relations of the Tabaquito batholith" section, abundant dykes were emplaced in the Tabaquito batholith. These dykes are part of the extensive Permian-Triassic magmatism of Frontal Cordillera called the Choiyoi group (see Llambías & Sato 1995; Rocher *et al*. 2015; Sato *et al.* 2015; del Rey *et al.* 2016). Geochronological and geochemical data suggest that these dykes can represent a subduction-related magmatism at 284 ± 4 Ma. The geochronological data reported here for the dykes and the Carboniferous granitoids strongly suggest that the Carboniferous magmatic arc was overprinted by the early Permian magmatic arc (Fig. 12C).

Summarising, we propose that the early Carboniferous and Permian magmatism results from a continuous subduction-related magmatic evolution, which continued until the present. The sequence of events agrees with the idealised tectonic evolution of an Andean orogenic cycle in which variations over time of the angle of subduction is the key factor controlling magmatic processes (Fig. 12), as was postulated by several authors (Alasino *et al.* 2012; Rocher *et al.* 2015; del Rey *et al.* 2016, Dahlquist *et al.* 2018a). Recently, del Rey *et al.* (2016) have postulated that the Andean subduction was a continuous process since the Middle Permian-Triassic (normally established since the Mesozoic). We conclude that the Andean magmatic cycle at this latitude might be extended to the Carboniferous time, where the arc environment was mostly continuous

from the early Carboniferous to the present, but marked by compositional changes in space and time in response to changes in the subduction angle of the oceanic plate.

Conclusions

The new Carboniferous SHRIMP U–Pb zircon age of 337 Ma obtained here along with previously published U-Pb data suggest that the Tabaquito batholith represents a long-lived magmatic plumbing system formed through at least two magmatic pulses, one at 337 Ma and other at 322 Ma, emplaced at shallow conditions (~750 ºC and 2 kbar). Furthermore, crystallisation and inherited ages (284 ± 4 Ma and 336 ± 3 Ma) of the studied mafic dyke suggest the superposition of Permian magmatism over the Carboniferous magmatism in this area.

Major and trace element compositions of the granodiorite, mafic enclave and sampled dykes are consistent with a subduction setting (continental arc). Chemical and mineralogical similarities of the studied rocks from the south and the north suggest the existence of a long-lived magmatic plumbing system of ca. 15 My, with the intrusion of younger batches into older crystal mushes.

Isotope composition of these rocks (εHf range –2.0 to +4.5; εNd_i range: –1.6 to −2.4; Sr/Sr_i: 0.7039−0.7071) might result from mixing of a mafic to intermediate end-member with a juvenile signature and a felsic end-member with a crustal signature (probably an older continental crust).

Comparison between Carboniferous arc-related granites from Chile and Argentina indicate the Argentine granites are enriched in K_2O. However, this K_2O enrichment does not seem to be related to a major involvement of the continental crust as suggested by isotope compositions.

Difference in age between the Argentine Carboniferous arc granitoids and their Chilean counterparts point to a migration of the magmatism toward the trench as a consequence of a change of the subduction angle. Accordingly, the Andean magmatic cycle can be extended to the Carboniferous time, where the arc setting would be continuous to the present and the compositional magma changes in space and time would be controlled by fluctuations of the subducting plate.

The widely recognised Carboniferous (ca. 350–340 Ma) magmatic event might suggest that South America, West Antarctica and New Zealand would have been part of the same subduction margin in an accretionary orogen developed in the SW Gondwana.

Acknowledgements

We dedicate this work to the memory of our beloved friend and colleague Professor Dr. Carmen Galindo. We are grateful to the staff of the Parque Nacional San Guillermo (San Juan Province, Argentina) for giving us the permissions to carry out the geological work in the park. Robert Stern is acknowledged for his valuable comments on an earlier version of the manuscript. We thank an anonymous reviewer and Rebecca A. VanderLeest for the thorough revision of the manuscript and for their insightful comments that have greatly improved the quality of the manuscript. We are also very grateful to Dr. Rooney for his efficient and helpful editorial handling as well as for his detailed comments and suggestions.

Funding information

Financial support for this paper was provided by Argentine public grants FONCyT PICT 2016 0843, PIP0178 CONICET, Spain public grant CGL2016-76439-P, and a stay developed by Juan A. Dahlquist in the Geosciences Institute of the Sao Paulo University supported by the grant FAPESP 2018/06837-3.

References

Abdel-Rahman, A.M. 1994. Nature of biotites from alkaline, calc-alkaline and peraluminous magmas. Journal of Petrology, 35, 525–541.

Alasino, P.H., Dahlquist, J.A., Pankhurst, R.J., Galindo, C., Casquet, C., Rapela, C.W., Larrovere, M. & Fanning, M. 2012. Early Carboniferous sub- to mid-alkaline magmatism in the Eastern Sierras Pampeanas, NW Argentina: A record of crustal growth by the incorporation of mantle-derived material in an extensional setting. Gondwana Research, 22, 992–1008.

Alasino, P.H., Casquet, C., Larrovere, M.A., Pankhurst, R.J., Galindo, C., Dahlquist, J.A., Baldo, E.G. & Rapela, C.W. 2014. Construction of a mid-crustal thermal aureole of Cerro Toro, Sierra de Famatina, NW Argentina. Lithos, 190–191, 154–172.

Alasino, P.H., Larrovere, M.A., Rocher, S., Dahlquist, J.A., Basei, M.A.S., Memeti, V., Paterson, S.R., Galindo, C., Macchioli Grande, M. & da Costa Campos Neto. M. 2017. Incremental growth of an upper crustal, A-type pluton, Argentina: evidence of a re-used magma pathway. Lithos, 284–285, 347–366.

Báez, M.A., Fogliata, A., Hagemann, S. & Santos, J.O. 2018. Magmatismo Carbonífero en la Sierra de Ambato, Catamarca, Argentina. Revista de la Asociación Geológica Argentina, 75(4), 601–608.

Bahlburg, H., Vervoort, J.D., Du Frane, S.A., Bock, B., Augustsson, C. & Reimann, R.C. 2009. Timing of crust formation and recycling in accretionary orogens: insights learned from the western margin of South America. Earth Science Reviews, 97, 227–253.

Caminos, R. 1972. El perfil geológico de la Cordillera entre los 28° 00′ y 28° 30′ de latitud sur, provincia de La Rioja, República Argentina. Revista de la Asociación Geológica Argentina, 27, 71–83.

Caminos, R.L. 1979. Cordillera Frontal. Segundo Simposio de Geología Regional Argentina. Academia Nacional de Ciencias Córdoba I, 398–453 (Córdoba).

Casquet C., Dahlquist J.A., Verdecchia S.O., Baldo E.G. Galindo C., Rapela C.W., Pankhurst R.J., Morales M.M., Murra J.A. & Fanning C.M. 2018. Review of the Cambrian Pampean orogeny of Argentina; a displaced orogeny formerly attached to the Saldania Belt of South Africa? Earth Science Reviews, 177, 209–225.

Cawood, P.A. 2005. Terra Australis Orogen: Rodinia breakup and development of the Pacific and Iapetus margins of Gondwana during the Neoproterozoic and Paleozoic. Earth-Science Reviews, 69, 249–279.

Chapman, J.B., Ducea, M.N., Kapp, P., Gehrels, G.E. & DeCelles, P.G. 2017. Spatial and temporal radiogenic isotopic trends of magmatism in Cordilleran orogens. Gondwana Research, 48, 189–204.

Chew, D.M., Schaltegger, U., Košler, J., Whitehouse, M.J., Gutjahr, M., Spikings, R.A. & Miškovic, A. 2007. U–Pb geochronologic evidence for the evolution of the Gondwanan margin of the north-central Andes. Geological Society of America Bulletin, 119, 697–711.

Clemens, J.D. & Stevens, G. 2012. What controls chemical variation in granitic magmas? Lithos, 134–135, 317–329.

Coira B., Cisterna C.E., Ulbrich H.H. & Cordani U.G. 2016. Extensional Carboniferous magmatism at the western margin of Gondwana: Las Lozas valley, Catamarca, Argentina. Andean Geology, 43, 105-126.

Coleman, D.S., Gray, W. & Glazner, A.F. 2004. Rethinking the emplacement and evolution of zoned plutons: Geochronologic evidence for incremental assembly of the Tuolumne Intrusive Suite, California. Geology, 32, 433–436.

Dahlquist, J.A. 2001. Low-pressure emplacement of epidote-bearing metaluminous granitoids in the Sierra de Chepes (Famatinian Orogen Argentina) and relationships with the magma sources. Revista Geológica de Chile, 28, 147–161.

Dahlquist, J.A., Pankhurst, R.J., Rapela, C.W., Galindo, C., Alasino, P., Fanning, C.M., Saavedra, J. & Baldo, E.G. 2008. New SHRIMP U–Pb data from the Famatina complex: constraining Early–Mid Ordovician Famatinian magmatism in the Sierras Pampeanas, Argentina. Geologica Acta, 6, 319–333.

Dahlquist, J.A., Alasino, P.H., Eby, G.N., Galindo, C. & Casquet, C. 2010. Fault controlled Carboniferous A-type magmatism in the proto-Andean foreland (Sierras Pampeanas, Argentina): Geochemical constraints and petrogenesis. Lithos, 115, 65–81.

Dahlquist, J.A., Pankhurst, R.J., Gaschnig, R.M., Rapela, C.W., Casquet, C., Alasino, P.H., Galindo, C. & Baldo, E.G. 2013. Hf isotopes in zircon and whole-rock Nd isotope composition as monitors of crustal growth in the proto-Andean margin of Gondwana: Early Ordovician to Early Carboniferous magmatism. Gondwana Research, 23, 1617–1630.

Dahlquist, J.A., Alasino, P.H. & Bello, C. 2014. Devonian aluminous A-type magmatism in the proto-Andean foreland (SierrasPampeanas, Argentina): geochemical constraints and petrogenesis of the Achala batholith. Mineralogy and Petrology, 108, 391–417.

Dahlquist, J.A., Morales Cámera, M.M. & Alasino, P.H. 2015. Petrografía, química mineral y geoquímica comparada de los plutones Potrerillos y Cerro La Gloria:

magmatismo de arco y retroarco en el carbonífero inferior. Revista de la Asociación Geológica Argentina, 72 (2), 167–181.

Dahlquist, J.A., Pankhurst, R.J., Rapela, C.W., Basei, M.A., Alasino,P.H., Saavedra, J., Baldo, E.G. Murra, J.A. & da Costa Campos Neto, M. 2016. The Capilla del Monte pluton, Sierras de Córdoba, Argentina: the easternmost Early Carboniferous magmatism in the pre-Andean SW Gondwana margin. International Journal of Earth Sciences, 105, 1287–1305.

Dahlquist, J.A., Alasino P.H., Basei, M.A.S., Morales Cámera, M., Macchioli Grandre, M. & Campos Neto, M.C. 2018a. Petrological, geochemical, isotopic, and geochronological constraints for the Late Devonian - Early Carboniferous magmatism in SW Gondwana (27−32 °LS): an example of geodynamic switching. International Journal of Earth Sciences. https://doi.org/10.1007/s00531-018-1615-9

Dahlquist, J.A., Alasino P.H., Basei, M.A.S., Morales Cámera, M., Macchioli Grandre, M., Campos Neto, M.C. & García Larrecharte, M. 2018b. Recurrent intrusive episodes in the Paleozoic metasedimentary upper crust during the Early Carboniferous time: The Veladero granitoid stock and the peraluminous andesite. Journal of South American Earth Sciences, 88, 88–93.

Dahlquist, J.A., Macchioli Grande, M., Alasino, P.H., Basei, M.A.S., Galindo, C., Moreno, J.A. & Morales Cámera, M.M. 2019. New geochronological and isotope data for the Las Chacras – Potrerillos and Renca batholiths: A contribution to the Middle-Upper Devonian magmatism in the pre-Andean foreland (Sierras Pampeanas, Argentina), SW Gondwana. Journal of South American Earth Sciences, 93, 348–363.

Deckart, K., Hervé, F., Fanning, M., Ramírez, V., Calderón, M. & Godoy, E. 2014.U–Pb geochronology and Hf–O isotopes of zircons from the Pennsylvanian Coastal Batholith, South-Central Chile. Andean Geology, 41, 49–82.

del Rey, A., Deckart, K., Arriagada, C. & Martínez, F. 2016. Resolving the paradigm of the late Paleozoic–Triassic Chilean magmatism: Isotopic approach. Gondwana Research, 7, 172–181.

DePaolo, D.J. 1981. Neodymium isotopes in the Colorado Front Range and implications for crust formation and mantle evolution in the Proterozoic. Nature, 291, 193–197.

Domeier M. & Torsvik T.H. 2014. Plate tectonics in the late Paleozoic. Geoscience Frontiers, 5, 303–350.

Ducea, M.N., Otamendi, J.E., Bergantz, G.W., Jianu, D. & Petrescu, L. 2015. The origin and petrologic evolution of the Ordovician Famatinian-Puna arc. En: DeCelles, P.G., Ducea, M.N., Carrapa, B., Kapp, P.A. (Eds.): Geodynamics of a cordilleran orogenic system: The Central Andes of Argentina and Northern Chile. Geological Society of America Memoir, 212, 125–138.

Evans, B.W. & Vance, J.A. 1987. Epidote phenocrysts in dacitic dikes, Boulder County, Colorado. Contributions to Mineralogy and Petrology, 96, 178–185.

Frigerio, P.V., Cingolani, C.A. & Chemale, Jr., F. 2012. El granito Potrerillos de la Precordillera de Jagüé, La Rioja: caracterización petrológica, geoquímica y geocronológica. Serie de Correlación Geológica, 28, 107–138.

Frost, B.R., Barnes, C.G., Collins, W.J., Arculus, R.J., Ellis, D.J. & Frost, C.D. 2001. A geochemical classification for granitic rocks. Journal of Petrology, 42, 2033–2048.

Gao, P., Zheng, Y.F. & Zhao, Z.F. 2016. Experimental melts from crustal rocks: a lithochemical constraint on granite petrogenesis. Lithos, 266-267, 133–157.

Glazner, A.F., Bartley, J.M., Coleman, D.S., Gray, W. & Taylor, R.Z. 2004. Are plutons assembled over millions of years by amalgamation from small magma chambers? GSA Today, 14, 4–11.

Grosse, P., Söllner, F., Báez, M.A., Toselli, A.J., Rossi, J.N., de la Rosa J.D. 2009. Lower carboniferous post-orogenic granites in central eastern Sierra de Velasco, Sierras Pampeanas, Argentina: U–Pb monazite geochronology and Sr–Nd isotopes. International Journal of Earth Sciences, 98, 1001–1025.

Hervé, F., Calderón, M., Fanning, C.M., Pankhurst, R.J. & Godoy, E. 2013. Provenance variations in the Late Paleozoic accretionary complex of central Chile as indicated by detrital zircons. Gondwana Research, 23, 1122–1135.

Hervé, F., Calderon, M., Fanning, C.M., Pankhurst, R.J., Fuentes, F., Rapela, C.W., Correa, J., Quezada, P. & Marambio, C. 2016. Devonian magmatism in the accretionary complex of southern Chile. Journal of the Geological Society (London), 173, 587–602.

Hildreth, W. & Moorbath, S. 1988. Crustal contributions to arc magmatism in the Andes of central Chile. Contributions to Mineralogy and Petrology, 98, 455–489.

Hines, R., Paterson, S.R., Memeti, V. & Chambers, J.A. 2018. Nested incremental growth of zoned upper crustal plutons in the Southern Uplands Terrane, UK: fractionating, mixing, and contaminated magma fingers. Journal of Petrology, 59, 483–516.

Holland, T. & Blundy, J. 1994. Non-ideal interactions in calcic amphiboles and their bearing on amphibole–plagioclase thermometry. Contributions to Mineralogy and Petrology, 116, 433–447.

Korhonen, F.J., Saito, S., Brown, M., Siddoway, C.S. & Day, J.M.D. 2010. Multiple generations of granite in the Fosdick Mountains, Marie Byrd Land, West Antarctica: implications for polyphase intracrustal differentiation in a continental margin setting. Journal of Petrology, 51, 627–670.

Larrovere, M.A., Alasino, P.A., de los Hoyos, C.R. & Willner, A.P. 2015. The Ordovician Las Chacritas pluton (Sierra de Humaya, NW Argentina): origin and emplacement triggered by lateral shortening and magmatic stoping at mid-crustal level. International Journal of Earth Sciences, 104, 565–586.

Leake, B.E. 1997. Nomenclature of amphiboles. Report of the Subcommittee on Amphiboles of the International Mineralogical Association Commission on the NewMineral Names. Canadian Mineralogist, 9, 623–651.

Leat, P.T., Storey, B.C. & Pankhurst, R.J. 1993. Geochemistry of Palaeozoic–Mesozoic Pacific rim orogenic magmatism, Thurston Island area, West Antarctica. Antarctic Science, 5, 281–296.

Lira, R., Millone, H.A., Kirschbaum, A.M. & Moreno, R.S. 1997. Calc-alkaline arc granitoid activity in the Sierra Norte-Ambargasta Ranges, Central Argentina. Journal of South American Earth Sciences, 10, 157–177.

Llambías, E.J. & Sato, A.M. 1990. El batolito de Colangüil (29º–31ºS) Cordillera Frontal de Argentina: estructura y marco tectónico. Revista Geológica de Chile, 17, 89–108.

Llambías, E.J. & Sato, A.M. 1995. El batolito de Colangüil: transición entre orogénesis y anorogénesis. Revista de la Asociación Geológica Argentina, 50 (1-4), 111–131.

Maksaev, V., Munizaga, F. & Tassinari, C. 2014. Timing of the magmatism of the paleo-Pacific border of Gondwana: U–Pb geochronology of Late Paleozoic to Early

Mesozoic igneous rocks of the north Chilean Andes between 20 degrees and 31 degrees S: Andean Geology 41, (3), 447–506.

Marsh, B.D. & Carmichael, I.S.E. 1974. Benioff zone magmatism. Journal of Geophysical Research, 79, 1196–206.

McDonough, W.F. & Sun, S.S. 1995. The composition of the Earth. Chemical Geology, 120, 223–253.

Millar, I.L., Pankhurst, R.J. & Fanning, C.M. 2002. Basement chronology of the Antarctic Peninsula: recurrent magmatism and anatexis in the Palaeozoic Gondwana margin. Journal of the Geological Society (London), 159, 145–157.

Miller, J.S., Matzel, J.E.P., Miller, C.F., Burgess, S.D. & Miller, R.B. 2007. Zircon growth and recycling during the assembly of large, composite arc plutons. Journal of Volcanology and Geothermal Research, 167, 282–299.

Mišković, A., Schaltegger, U., Spikings, R.A., Chew, D.M. & Košler, J. 2009. Tectono-magmatic evolution of western Amazonia: geochemical characterisation and zircon U–Pb geochronologic constraints from the Peruvian Eastern Cordilleran granitoids. Geological Society of America Bulletin, 121, 1298–1324.

Molina, J.F., Scarrow, J.H., Montero, P. & Bea, F. 2009. High-Ti amphibole as a petrogenetic indicator of magma chemistry: evidence for mildly alkalic-hybrid melts during evolution of Variscan basic–ultrabasic magmatism of Central Iberia. Contributions to Mineralogy and Petrology, 158, 69–98.

Molina, J.F., Moreno, J.A., Castro, A., Rodríguez, C. & Fershtater, G.B. 2015. Calcic amphibole thermobarometry in metamorphic and igneous rocks: new calibrations based on plagioclase/amphibole Al-Si partitioning and amphibole/liquid Mg partitioning. Lithos, 232, 286–305.

Morales Cámera, M., Dahlquist, J.A., Basei, M.A.S., Galindo, C., Campos Neto, M.C. & Facetti, N. 2017. F-rich strongly peraluminous A-type magmatism in the pre-Andean foreland Sierras Pampeanas, Argentina: Geochemical, geochronological, isotopic constraints and petrogenesis. Lithos, 277, 210–227.

Morales Cámera, M.M., Dahlquist, J.A., Ramacciotti, C.D., Galindo, C., Basei, M.A., Zandomeni, P.S. & Grande, M.M. 2018. The strongly peraluminous A-type granites of the Characato suite (Achala batholith), Sierras Pampeanas, Argentina: Evidence of Devonian-Carboniferous crustal reworking. Journal of South American Earth Sciences, 88, 551–567.

Moreno, J.A., Molina, J.F., Montero, P., Abu Anbar, M., Scarrow, J.H., Cambeses, A. & Bea, F. 2014. Unraveling sources of A-type magmas in juvenile continental crust: constraints from compositionally diverse Ediacaran post-collisional granitoids in the Katerina Ring Complex, southern Sinai, Egypt. Lithos, 192–195, 56–85.

Moreno, J.A., Molina, J.F., Bea, F., Abu Anbar, M. & Montero, P. 2016. Th-REE- and Nb-Ta-accessory minerals in post-collisional Ediacaran felsic rocks from the Katerina Ring Complex (S. Sinai, Egypt): an assessment for the fractionation of Y/Nb, Th/Nb, La/Nb and Ce/Pb in highly evolved A-type granites. Lithos, 258–259, 173–196.

Mutch, E.J.F., Blundy, J.D., Tattitch, B.C., Cooper, F.J. & Brooker, R.A. 2016. An experimental study of amphibole stability in low-pressure granitic magmas and a revised Al-in-hornblende geobarometer. Contributions to Mineralogy and Petrology, 171, 1–27.

Nasi, C., Mpodozis, C., Cornejo, P., Moscoso, R. & Maksaev, V. 1985. El Batolito Elqui-Limarí (Paleozoico Superior-Triásico): características petrográficas, geoquímicasy significado tectónico. Revista Geológica de Chile, 25–26, 77–11.

Otamendi, J.E., Ducea, M.N., Cristofolini, E.A., Tibaldi, A.M., Camilletti, G.C. & Bergantz, G.W. 2017. U–Pb ages and Hf isotope compositions of zircons in plutonic rocks from the central Famatinian arc, Argentina. Journal of South American Earth Sciences, 76, 412–426.

Pankhurst, R.J. & Rapela, C.W. 1998. The proto-Andean margin of Gondwana: an introduction. In: Pankhurst, R.J., Rapela, C.W. (Eds.), Geological Society, London, Special Publications, 142, 1–9.

Pankhurst, R.J., Millar, I.L., Grunow, A.M. & Storey, B.C. 1993. The pre-Cenozoic magmatic history of the Thurston Island crustal block, West Antarctica. Journal of Geophysical Research - Solid Earth, 98, 11 835–11 849.

Pankhurst, R.J., Weaver, S.D., Bradshaw, J.D., Storey, B.C. & Ireland, T.R. 1998. Geochronology and geochemistry of pre-Jurassic superterranes in Marie Byrd Land, Antarctica. Journal of Geophysical Research, 103, 2529–2547.

Pankhurst, R.J., Rapela, C.W., Fanning, C.M. & Marquez, M. 2006. Gondwanide continental collision and the origin of Patagonia. Earth-Science Reviews, 76, 235–257.

Parada, M.A., Munizaga, F. & Kawashita, K. 1981. Edades Rb-Sr roca total del bato lito compuesto de los ríos Elqui-Limarí en la latitud 300 S. Revista Geológica de Chile, 13–14, 87–93.

Parada, M.A., Nystrom, J.O. & Levi, B. 1999. Multiple sources for the Coastal Batholith of central Chile (31–34°S): geochemical and Sr–Nd isotopic evidence and tectonic implications. Lithos, 46, 505–521.

Paterson, S.R., Memeti, V., Mundil, R. & Žák, J. 2016. Repeated, multiscale, magmatic erosion and recycling in an upper crustal pluton: implications for magma chamber

dynamics and magma volume estimates, In: Special collection: perspectives on origins and evolution of crustal magmas. American Mineralogist, 101, 2176–2198.

Pitcher, W.S. 1993. The nature and origin of granite. London, Blackie, 321 p.

Putirka, K. 2016. Amphibole thermometers and barometers for igneous systems, and some implications for eruption mechanisms of felsic magmas at arc volcanoes. American Mineralogist, 101, 841–858.

Quartino, B.J. & Zardini, R.A. 1967. Geología y petrología de la Cordillera de Colangüil y las serranías de Santa Rosa y San Guillermo, Cordillera Frontal de San Juan. Revista de la Asociación Geológica Argentina, 22, 5–63.

Ridolfi, F. & Renzulli, A. 2012. Calcic amphiboles in calc-alkaline and alkaline magmas: thermobarometric and chemometric empirical equations valid up to 1130 ºC and 2.2 GPa. Contributions to Mineralogy and Petrology, 163, 877–895.

Riley, T.R., Flowerdew, M.J., Pankhurst, R.J., Leat, P.T., Millar, I.L., Fanning, C.M. & Whitehouse, M.J. 2017. A revised geochronology of Thurston Island, West Antarctica, and correlations along the proto-Pacific margin of Gondwana. Antarctic Science, 29, 47–60.

Rocher, A., Vallecillo, G.M., Castro de Machuca, B. & Alasino, P. 2015. El Grupo Choiyoi (Pérmico temprano-medio) en la Cordillera Frontal de Calingasta, San Juan, Argentina: volcanismo de arco asociado a extensión. Revista Mexicana de Ciencias Geológicas, 32, 415–432.

Sato, A.M., Llambías, E., Basei, M. & Castro, E. 2015. Three stages in the Late Paleozoic to Triassic magmatism of southwestern Gondwana, and the relationships with the volcanogenic events in coeval basins. Journal of South American Earth Sciences, 63, 48–69.

Schmidt, M.W. 1992. Amphibole composition in tonalite as a function of pressure: an experimental calibration of the aluminium-in-hornblende barometer. Contributions to Mineralogy and Petrology, 110, 304–310.

Siégel, C., Bryan, S.E., Allen, C.M. & Gust, D.A. 2018. Use and abuse of zircon-based thermometers: a critical review and a recommended approach to identify antecrystic zircons. Earth Science Reviews, 176, 87–116.

Siegesmund, S., Steenken, A., López de Luchi, M.G., Wemmer, K., Hoffmann, A. & Mosch, S. 2004. The Las Chacras-Potrerillos batholith (Pampean Ranges, Argentina): structural evidence, emplacement and timing of the intrusion. International Journal of Earth Sciences, 93, 23–43.

Stern, R.J. 2002. Crustal evolution in the East African Orogen: a neodymium isotopic perspective. Journal of African Earth Sciences, 34, 109–117.

Tischendorf, G., Rieder, M., Förster, H.-J., Gottesmann, B. & Guidotti, C.V. 2004. A new graphical presentation and subdivision of potassium micas. Mineralogical Magazine, 68, 649–667.

Tischendorf, G., Förster, H.-J., Gottesmann, B. & Rieder, M. 2007. True and brittle micas: composition and solid-solution series. Mineralogical Magazine, 71, 285–320.

Tulloch, A.J., Ramezani, J., Kimbrough, D.L., Faure, K., & Allibone, A.H. 2009. U-Pb geochronology of mid-Paleozoic plutonism in western New Zealand; implications for S-type granite generation and growth of the east Gondwana margin: Geological Society of America Bulletin, 121, 1236–1261.

Von Gosen, W., McClelland, W.C., Loske, W., Martínez, J.C. & Prozzi, C. 2014. Geochronology of igneous rocks in the Sierra Norte de Córdoba (Argentina):

Implications for the Pampean evolution at the western Gondwana margin. Lithosphere, 6, 277–300.

Vyhnal, C.R., McSween, H.Y. & Speer, J.A. 1991. Hornblende chemistry in southern Appalachian granitoids: implications for aluminium hornblende thermobarometry and magmatic epidote stability. American Mineralogist, 76, 176–188.

Willner, A.P., Gerdes, A., Massonne, H.J., Schmidt, A., Sudo, M., Thomson, S.N. & Vujovich, G. 2011. The geodynamics of collision of a microplate (Chilenia) in Devonian times deduced by the pressure–temperature–time evolution within part of a collisional belt (Guarguaraz Complex,W-Argentina). Contributions to Mineralogy and Petrology, 162, 303–327.

Yakymchuk, C., Brown, C.R., Brown, M., Siddoway, C.S., Fanning, C.M. & Korhonen, F.J. 2015. Paleozoic evolution of western Marie Byrd Land, Antarctica. Geological Society of America Bulletin, 127, 1464–1484.

Young, A., Flament, N., Maloney, K., Williams, S., Matthews, K., Zahirovic, S. & Müller, R. D. 2019. Global kinematics of tectonic plates and subduction zones since the late Paleozoic Era. Geoscience Frontiers, 10, 989–1013.

Figure captions

Fig. 1. Schematic regional geological map of Central NW Argentina (modified after Dahlquist et al. 2018a) and the location of the studied area. The dashed line is the suggested boundary between arc and retro-arc magmatism. Reprinted by permission from: Springer Nature, International Journal of Earth Sciences, Dahlquist *et al.* 2018a.

Fig. 2. Simplified geological map of the Tabaquito batholith. The batholith has plenty of dykes but mapping them was not part of this work. Grey lines are schematic representations of some dykes. Stars represent location of the studied samples. In the boxes close to each star it is indicated the samples collected in that area. Samples collected for this study are indicated with black text whereas a sample collected by Dahlquist et al. (2018a) is highlighted in blue.

Fig. 3. Field photographs. (A) Decimetre-scale mafic microgranular enclave included in the Tabaquito granodiorite. (B) Panoramic view of the intrusive contact between the Tabaquito batholith and metasedimentary rocks of the Chinguillos Formation. (C) Decimetre- to centimetre-scale country rock xenoliths enclosed in the Tabaquito granodiorite close to the contact. (D) Metre-scale outcrop of a fine-grained biotite leucogranite within the Tabaquito granodiorite, which encompass the rest of the outcrops and the cover observed in the photography. (E) Panoramic view of the porphyritic granite and the Tabaquito granodiorite located in the southern sector of the batholith. The dashed line marks the inferred contact. (F) Aplitic dyke intruding the porphyritic granite. The white dashed line represents contact between the dyke and the porphyritic granite. Abbreviations: AD, aplitic dyke; CF, Chinguillos Formation; MME, mafic microgranular enclave; PG, porphyritic granite; TG, Tabaquito granodiorite.

Fig. 4. Composition of feldspar, biotite and amphibole from the Tabaquito granitoids. A) Feldspar composition. An–Ab–Or diagram (data in mol.%). B) Biotite composition. Feal vs. mgli diagram (after Tischendorf et al. 2007). Hollow circles represent end-member compositions that are indicated with abbreviations. C) Biotite composition. Al_2O_3 vs. SiO_2 and MgO–FeO–Al_2O_3 diagram (after Abdel-Rahman, 1994). Data in wt.%. D) Calcic amphibole composition. Mg number vs. Si diagram. Abbreviations: Ab, albite; An, anorthite; Ann, annite; Cel, celadonite; Eas, eastonite; Hyp-mus, hyper-muscovite; Mus, muscovite; Mont, montdorite; Phl, phlogopite; Pol, polylithionite; Or, orthoclase; Sid, siderophyllite; Tri, trilithionite.

Fig. 5. Tera-Wasserburg plots of samples TAB-24 (A) and TAB-40 (B). Figure (B) shows two zircon populations based on their ages, where green circles represent crystallization ages and blue circles represent inherited zircons.

Fig. 6. Whole-rock composition of the Tabaquito granitoids. (A) Fe-number vs. SiO_2 diagram. Cordilleran granitoid field (light blue) after Frost et al. (2001). (B) MALI-index vs. SiO_2 diagram after Frost et al. (2001). (C) Molar alumina saturation index vs. $Al_2O_3/(Na_2O + K_2O)$. (D) SiO_2 vs. K_2O diagram. (E) TAS (Total Alkali Silica) diagram. Data of the Carboniferous subduction related magmatism from Argentina (Frontal Cordillera and Western Sierras Pampeanas) and Chile are taken from Nasi *et al.* (1985), Parada *et al.* (1999) and Dahlquist *et al.* (2018a).

Fig. 7. Chondrite-normalised REE and Silicate Earth-normalised trace element diagrams. Normalisation values after McDonough & Sun (1995). Orange field shows composition of the Argentine Carboniferous arc-related granitoids (after Dahlquist *et al.* 2018a). Blue line delimitates the compositional field of the Carboniferous I-type rocks from Patagonia (Pankhurst et al. 2006).

Fig. 8. Relationships of trace-elements ratios of the Tabaquito granitoids. (A) $(Th/Nb)_N$ vs. $(Y/Nb)_N$. (B) $(Th/Nb)_N$ vs. $(La/Nb)_N$. Normalisation values after McDonough & Sun (1995). Compositional fields after Moreno *et al.* (2016). Abbreviations: CA, Continental Arcs; CC, Continental Crust; IA, Island Arcs; OIB, Ocean Island Basalts; Sh, shoshonites; Sub, subduction-related magmatic suites.

Fig. 9. (A)Tera-Wasserburg Concordia plot of sample TAB-11. (B) Weighted mean diagram of sample TAB-11 (data from supplementary file 2 in Dahlquist *et al.* 2018a). Zircon analyses with ages between 330 and 347 Ma are shown in green. Insets show the calculated Concordia and weighted mean ages.

Fig. 10. Regional map showing time and space distribution of the Carboniferous magmatism between 27ºS latitude and 34ºS latitude. A-type retro-arc magmatism in orange and arc magmatism in red. Geochronological data taken from Deckart *et al.* (2014), Maksaev *et al.* (2014), del Rey *et al.* (2016), Dahlquist *et al.* (2018a), Báez *et al.* (2018) and Morales Cámera *et al.* (2018). Blue text indicates the new U-Pb ages from this study. The different shade of yellow in the boxes differentiate the various age ranges (light yellow: 307-337 Ma; yellow: 340-357 Ma; yellow orange: 359-393 Ma).

Fig. 11. Reconstruction of the western margin of Gondwana at 340 Ma from Young *et al.* (2019). Purple lines with triangles on the overriding plate indicate subduction zones, and blue lines denote mid-ocean ridges and transform faults. The numbers indicate regions in which Carboniferous calc-alkaline I-types granitic rocks have been reported. See text for discussion and references. Figure was constructed using GPlates (www.gplates.org).

Fig. 12. Schematic geodynamic model showing the possible fluctuation of the subduction angle of the oceanic plate. Red colour indicates Carboniferous magmas and pink colour indicates Permian magmas.

Table captions

Table 1. *U-Pb SHRIMP data for igneous zircon from samples TAB-24 and TAB-40.*

Table 2. *Whole-rock compositions from the Tabaquito granitoids and dykes.*

Table 3. *Summary of P–T conditions in mineral assemblages from the Tabaquito granitoids.*

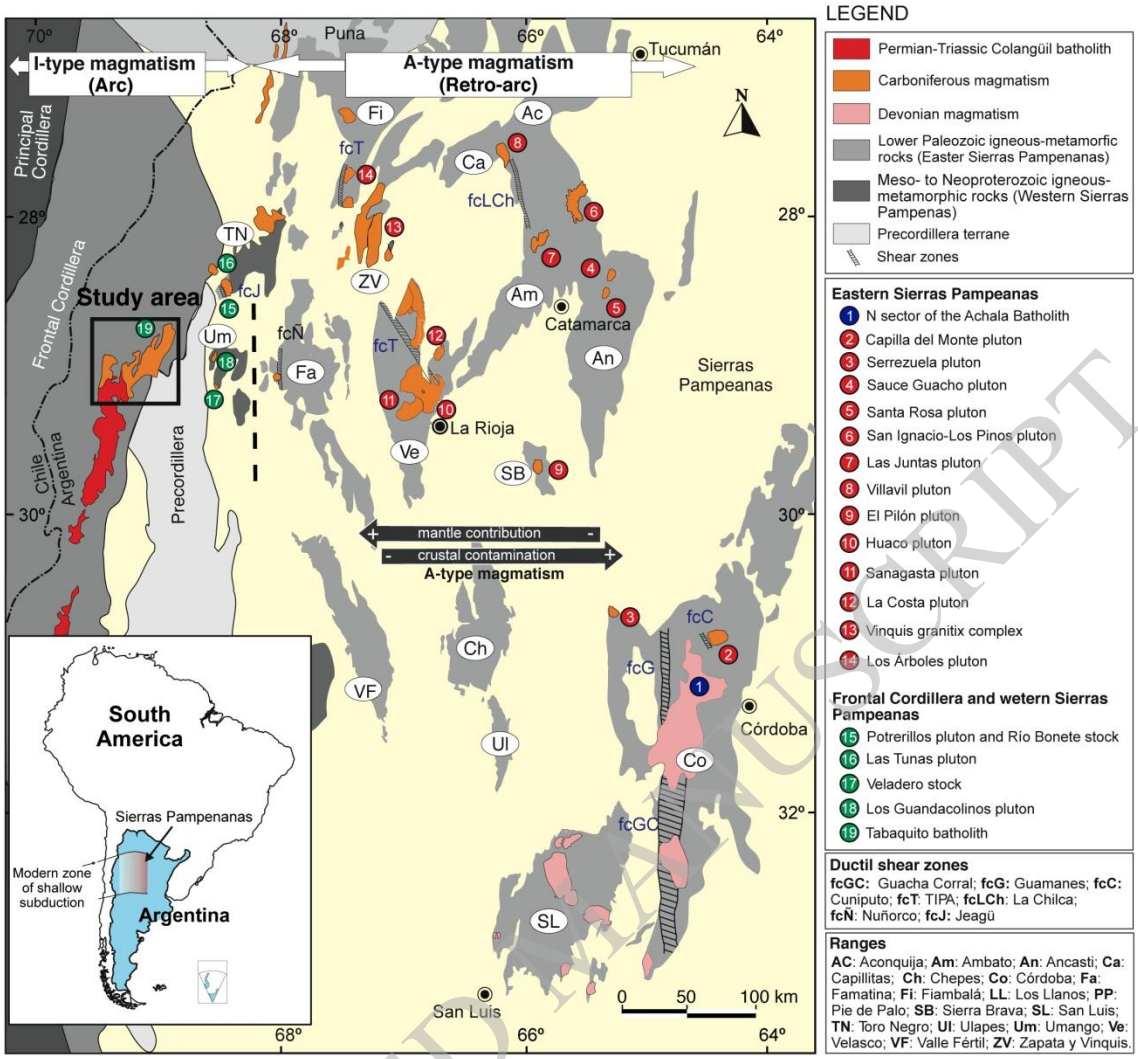

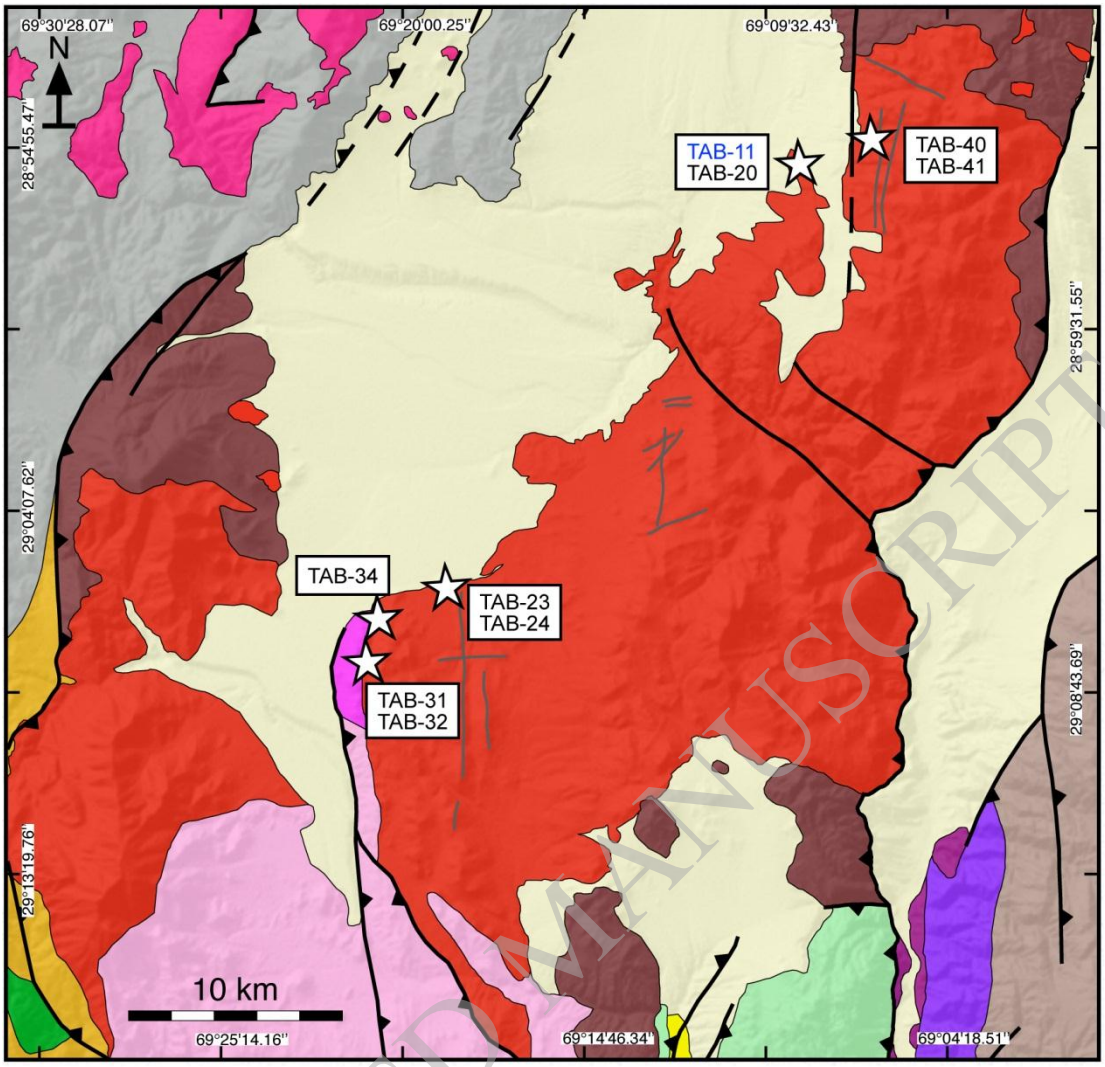

Cenozoic undifferentiated sedimentary rocks and deposits

Paleogene volcanosedimentary sequences

Triassic Santo Domingo Fm

Permian-Triassic plutonic and volcanic rocks

Coarse-grained porphyritic granite

Permian Los Puentes granite

Carboniferous Tabaquito batholith

Carboniferous undifferentiated sedimentary and volcanic rocks

Carboniferous Agua Negra Fm

Devonian/Carboniferous Punilla Fm

Devonian Chinguillos Fm

Ordovician Rio Blanco Fm

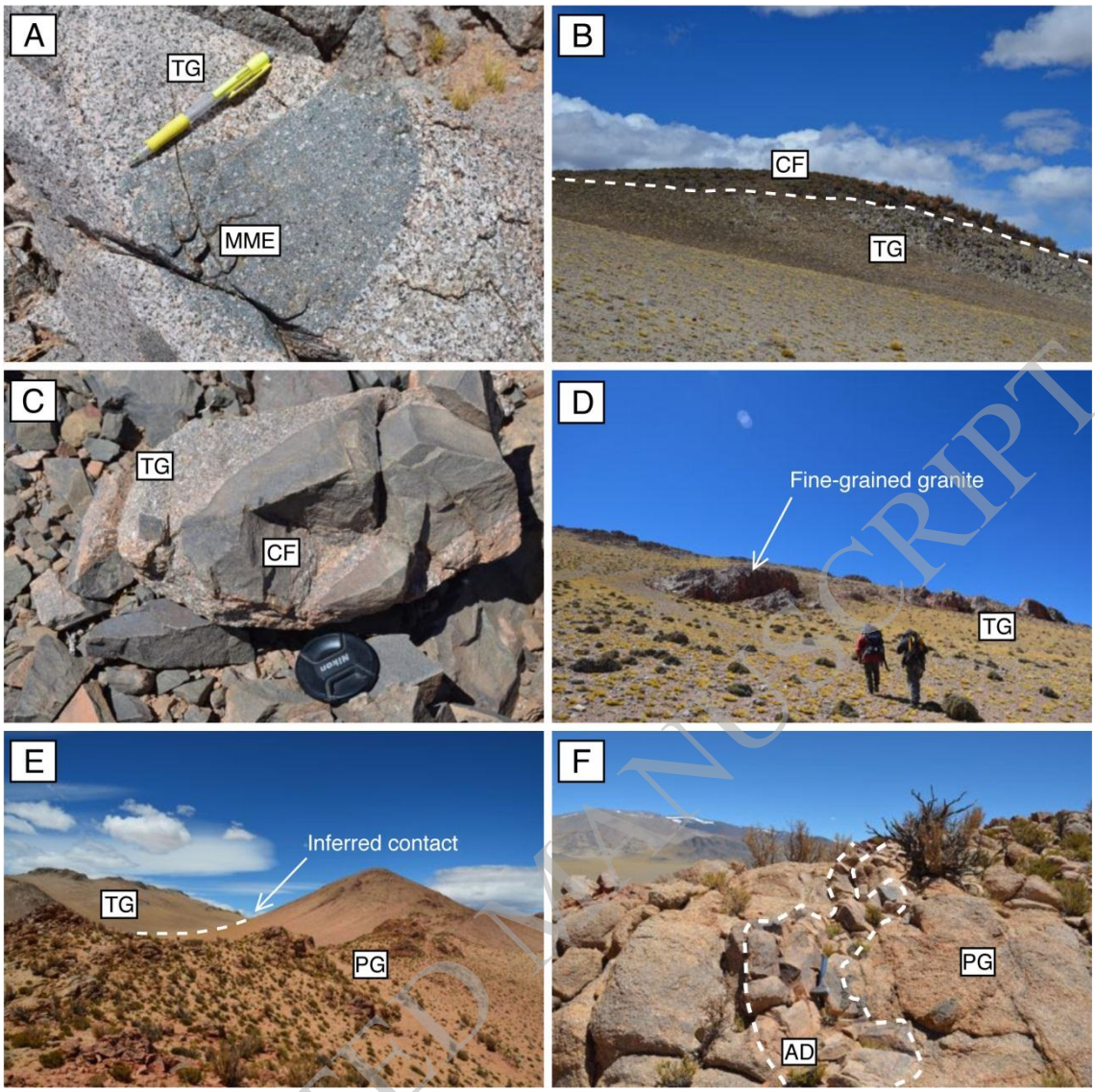

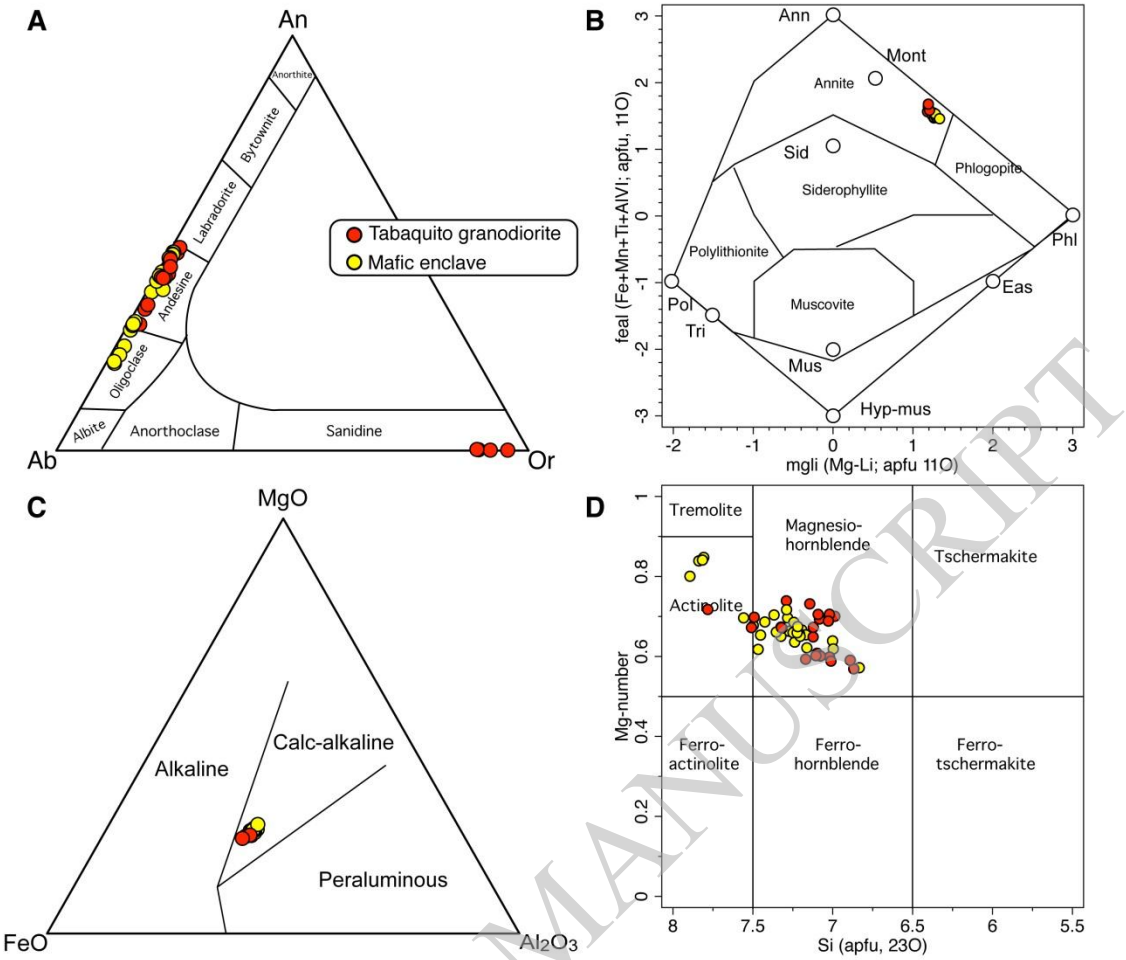

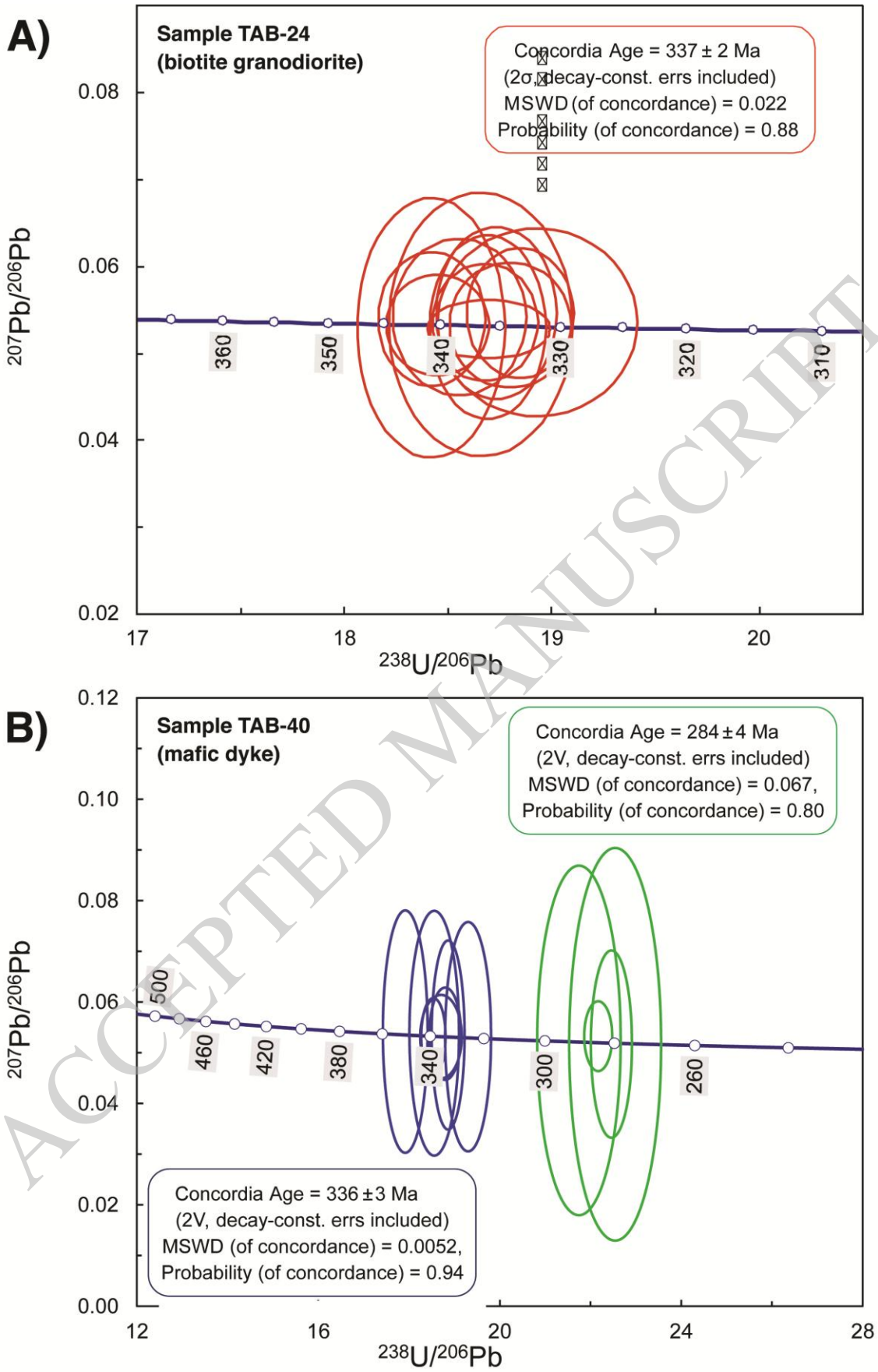

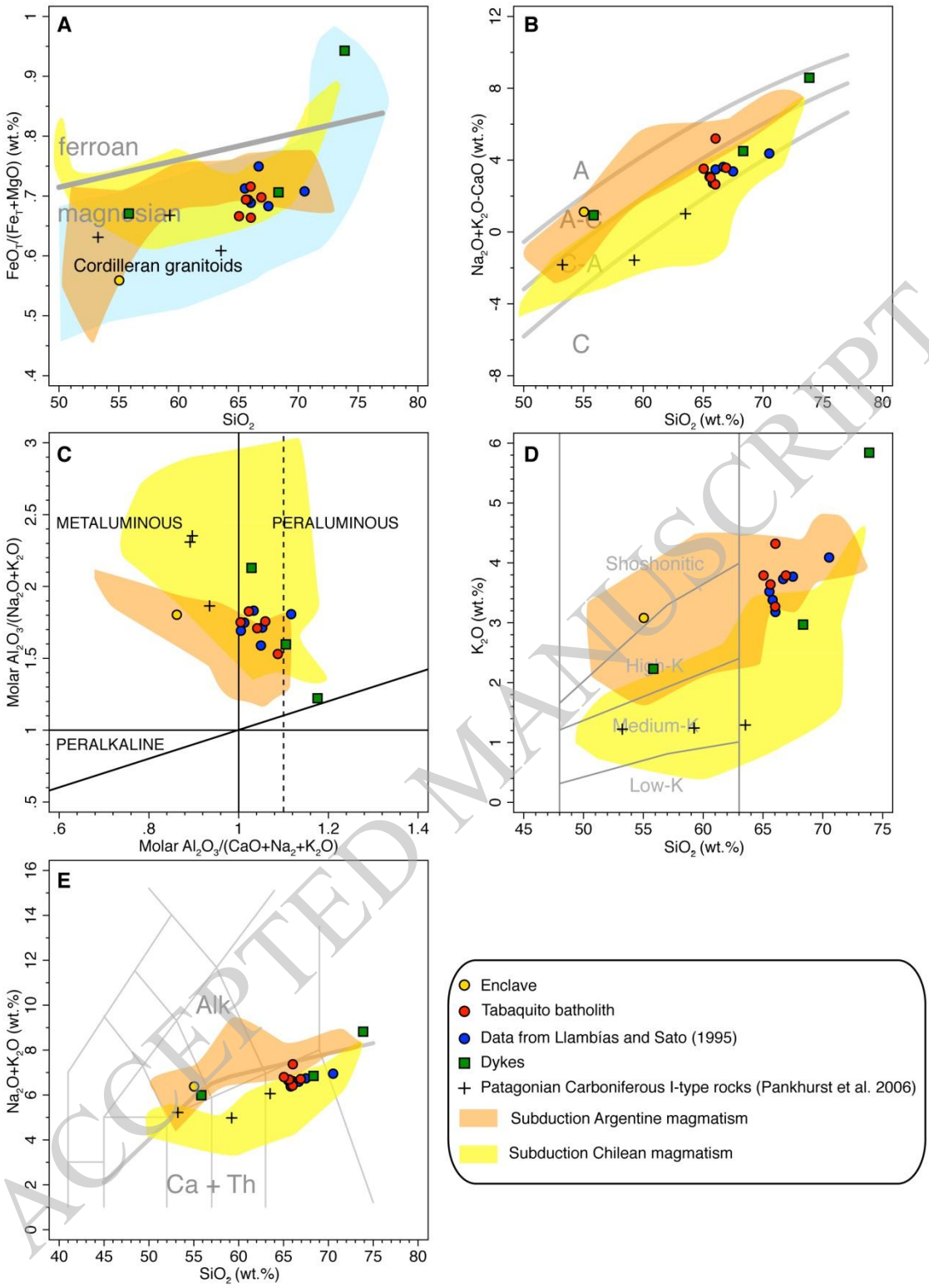

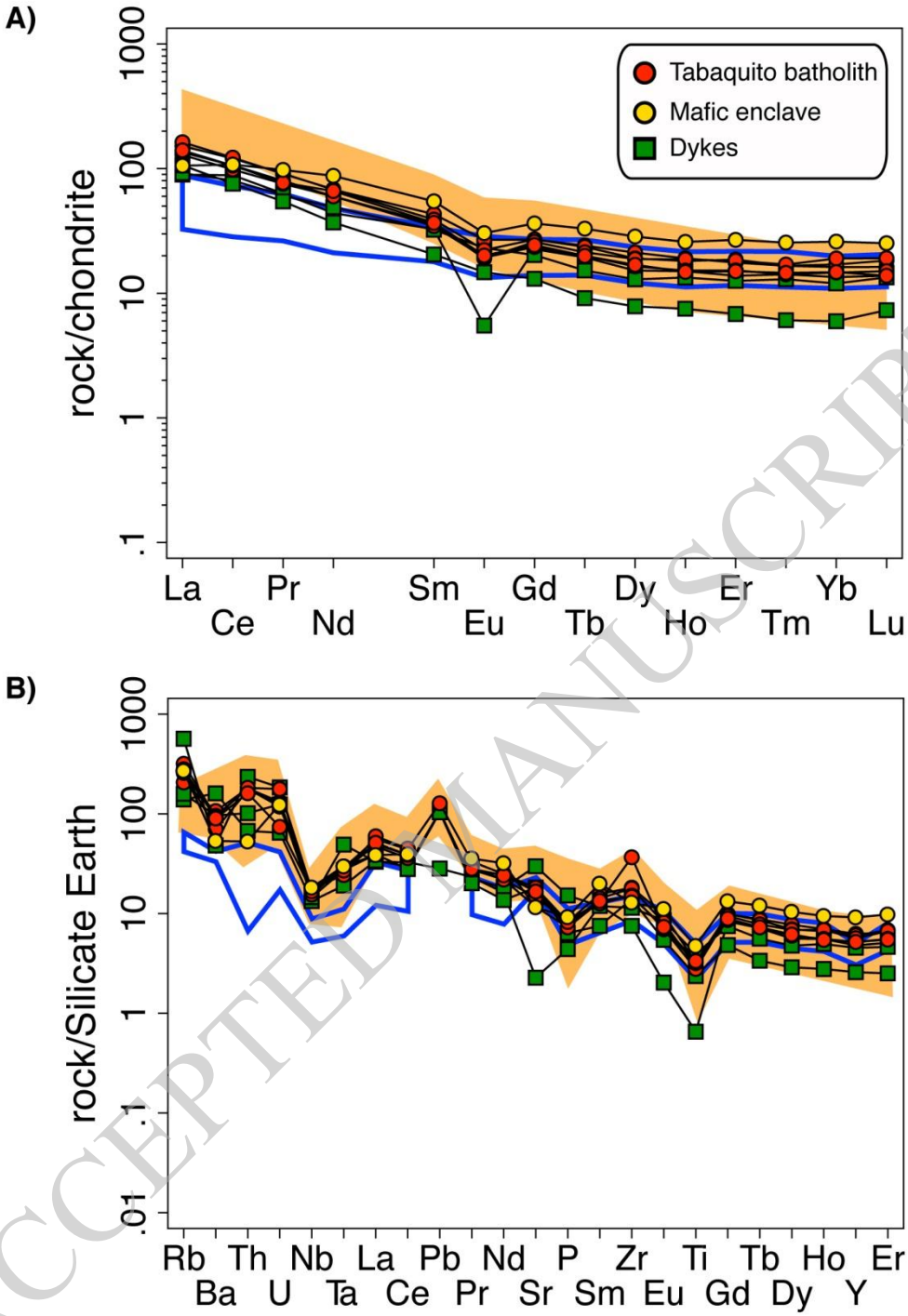

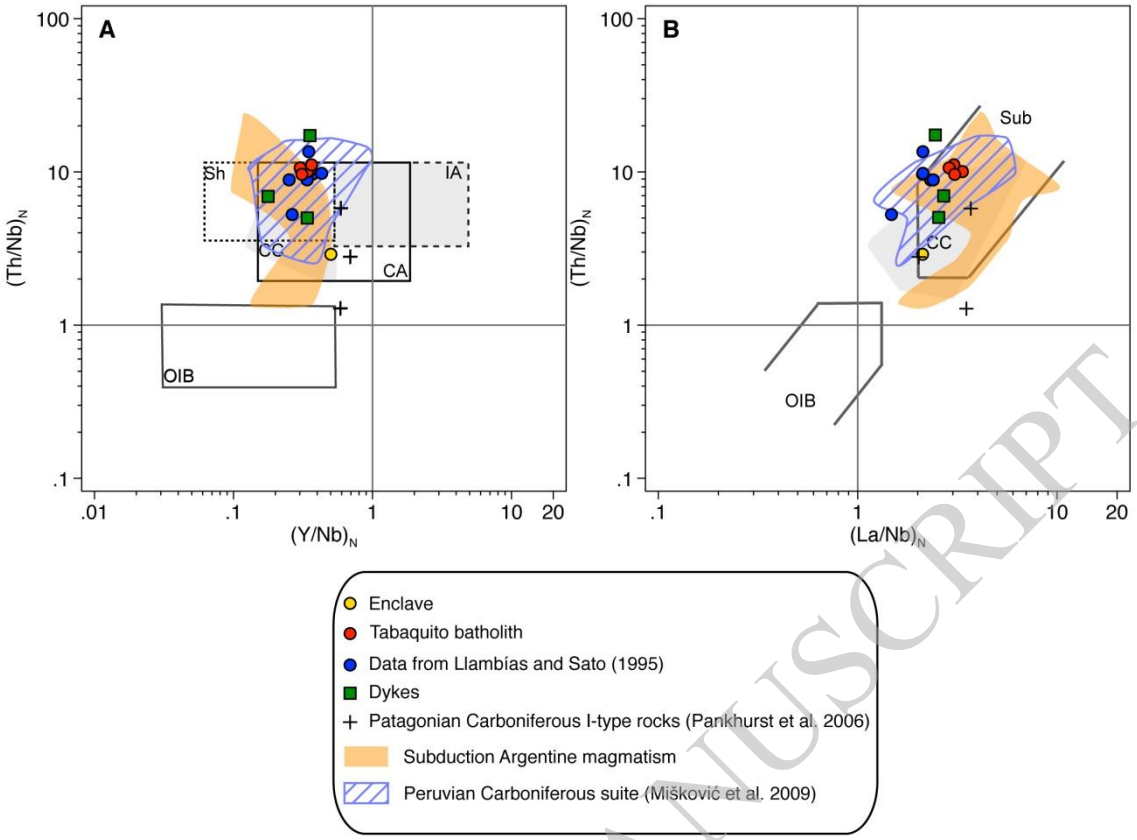

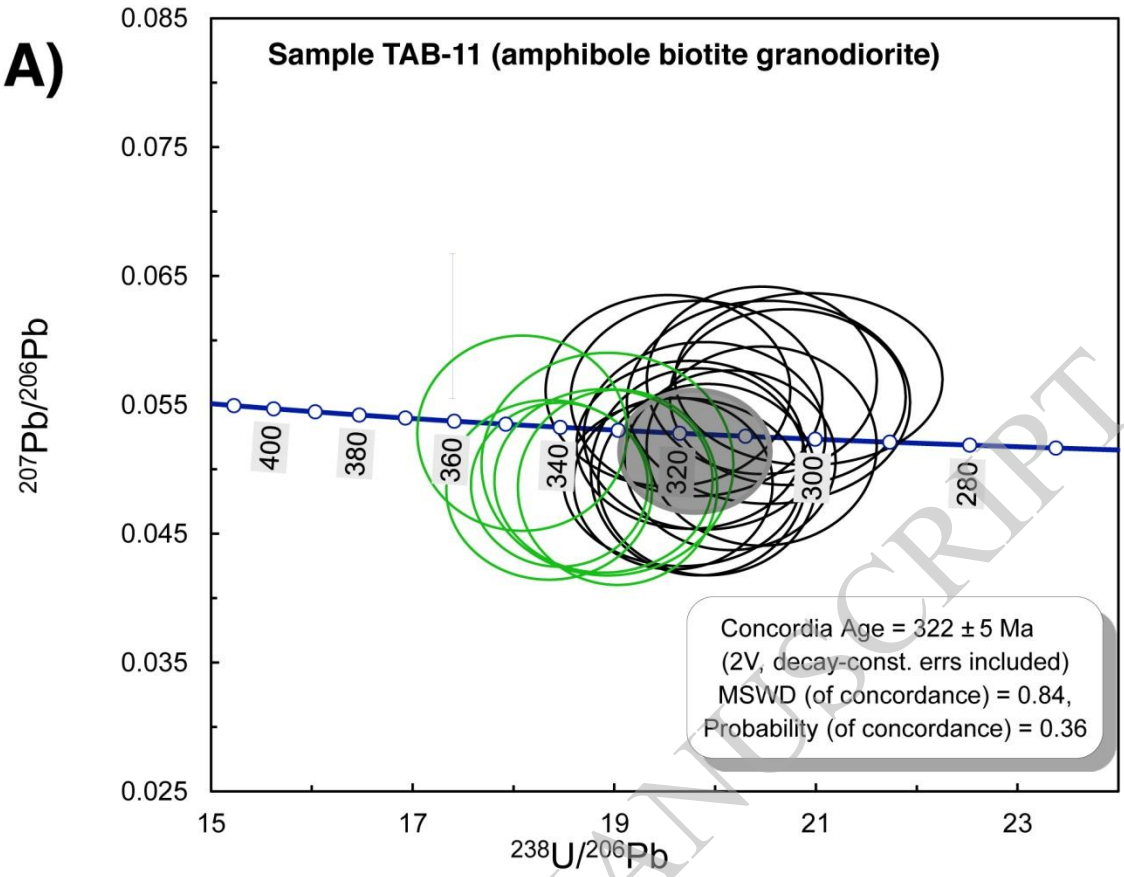

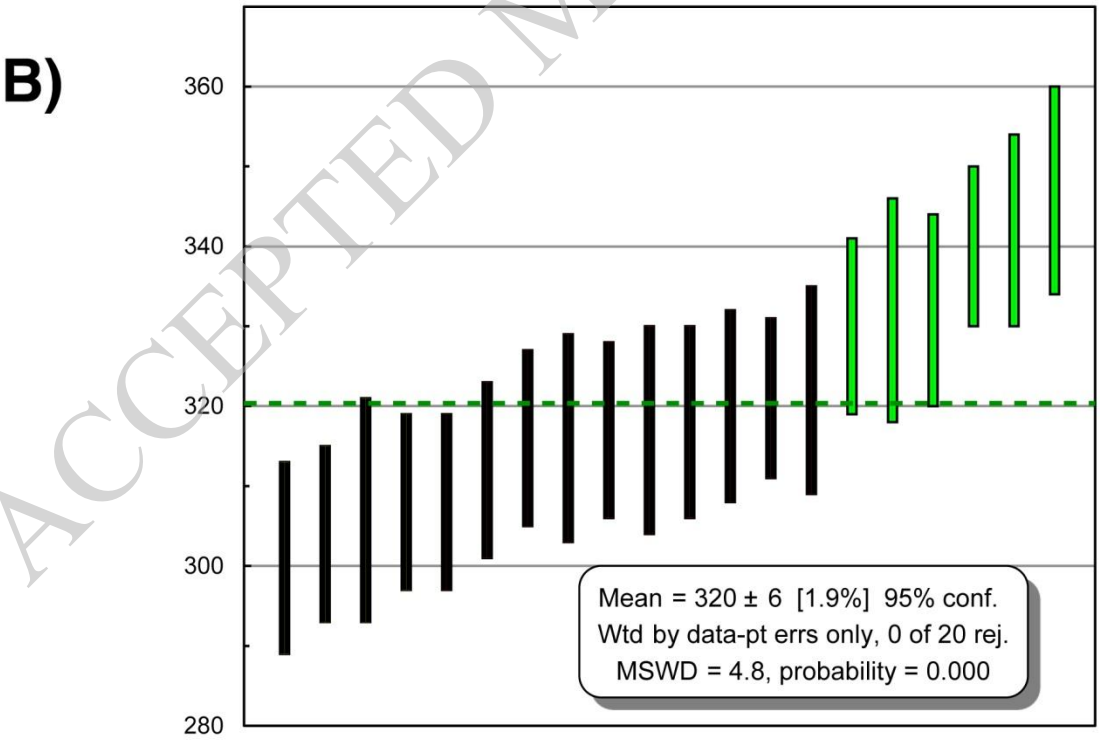

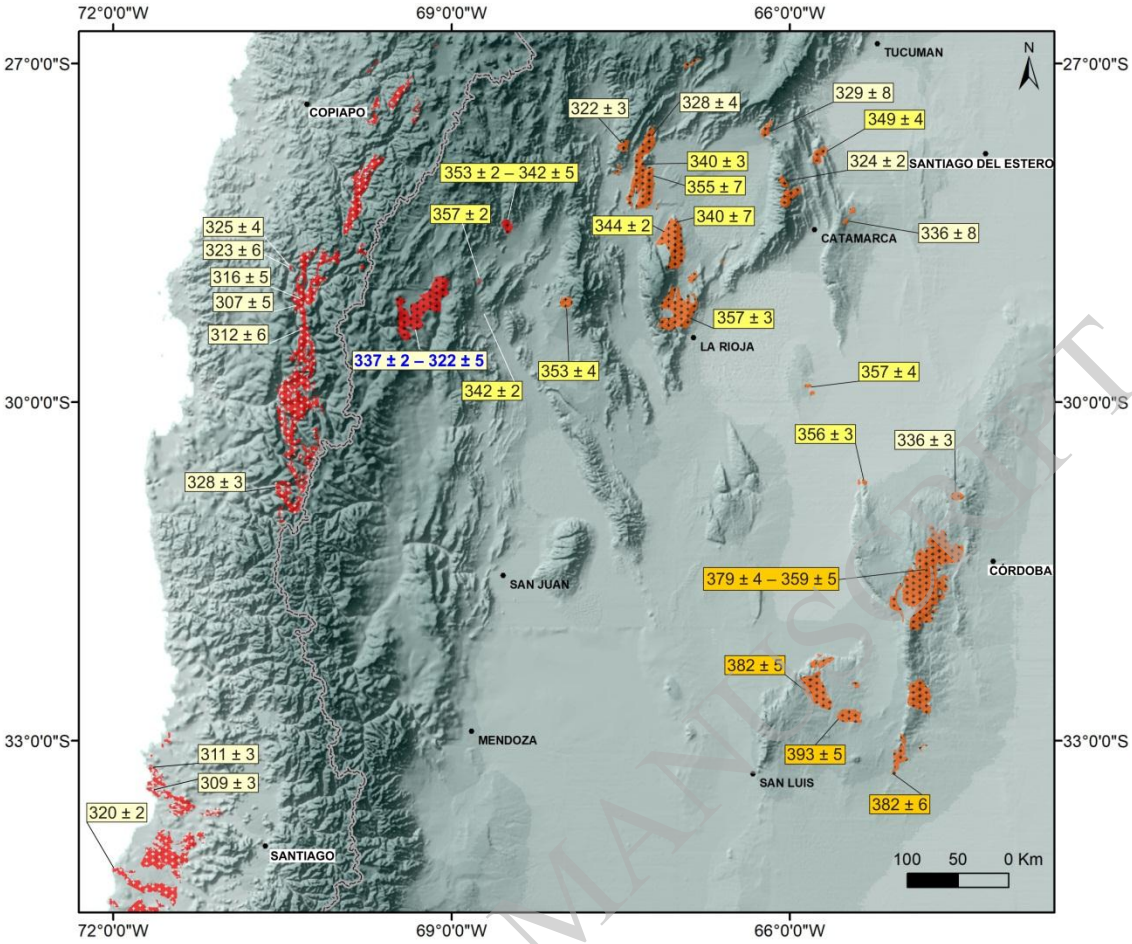

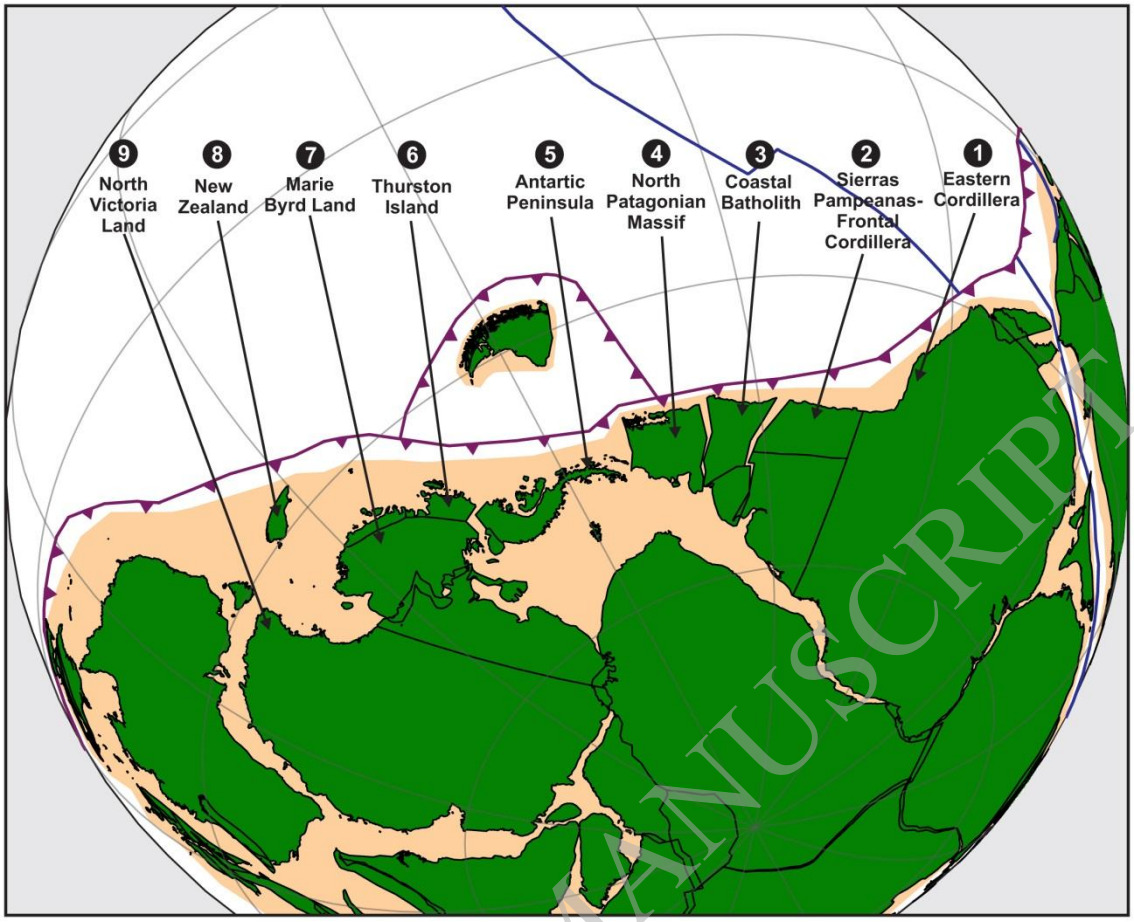

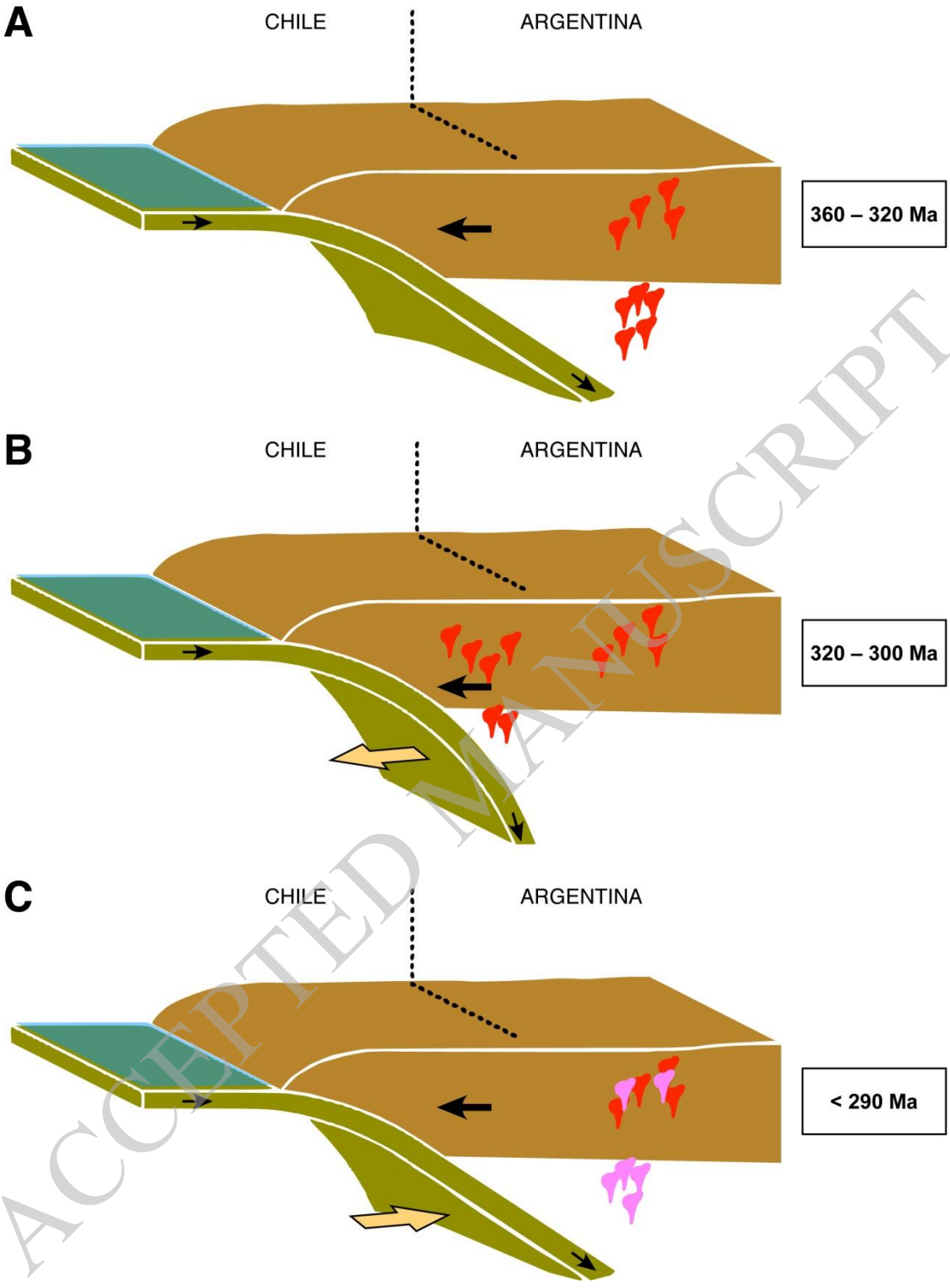

Table 1. *U-Pb SHRIMP data for igneous zircon from samples TAB-24 and TAB-40.*

Grain spot	GCh SS	U (ppm)	Th (ppm)	Th/U	$^{206}Pb_c$ (ppm)	$^{204}Pb/^{206}Pb$	f_{206} %	Total Ratios				Radiogenic Ratios*									Radiogenic Age (Ma)				
								$^{238}U/^{206}Pb$	±	$^{207}Pb/^{206}Pb$	±	$^{238}U/^{206}Pb$	±	$^{207}Pb/^{206}Pb$	±	$^{207}Pb/^{235}U$	±	$^{206}Pb/^{238}U$	±	rho	$^{206}Pb/^{238}U$	±	$^{207}Pb/^{206}Pb$	±	% Disc
Sample TAB-24																									
1.1	e,p,osc	446	55	0.12	20.3	1.1E-3	1.95	18.48	0.2	0.0700	0.0042	18.84	0.1717	0.05461	0.0049	0.400	0.0364	0.0531	0.0005	0.10	333	3	396	203	+16
2.1	c,p,osc	309	76	0.25	14.2	1.7E-3	3.09	18.15	0.2	0.0790	0.0052	18.73	0.1909	0.05471	0.0066	0.403	0.0486	0.0534	0.0005	0.08	335	3	400	269	+17
3.1	c,p,osc	519	76	0.15	23.7	1.3E-3	2.35	18.36	0.2	0.0720	0.0040	18.80	0.1936	0.05331	0.0048	0.391	0.0353	0.0532	0.0005	0.11	334	3	342	203	+2
4.1	e,p,osc	519	138	0.27	23.9	1.1E-3	1.96	18.31	0.2	0.0690	0.0038	18.67	0.1678	0.05360	0.0045	0.396	0.0334	0.0535	0.0005	0.11	336	3	354	189	+5
5.1	e,p,osc	329	98	0.30	15.3	1.7E-3	3.09	17.84	0.2	0.0780	0.0064	18.41	0.2353	0.05295	0.0099	0.397	0.0740	0.0543	0.0007	0.07	341	4	327	423	-4
6.1	e,p,osc	328	79	0.24	15.1	1.7E-3	3.01	18.13	0.2	0.0770	0.0059	18.69	0.1849	0.05311	0.0070	0.392	0.0518	0.0535	0.0005	0.07	336	3	334	299	-1
7.1	c,p,osc	262	82	0.31	12.1	2.8E-3	5.15	17.69	0.3	0.0950	0.0079	18.65	0.2923	0.05333	0.0100	0.394	0.0745	0.0536	0.0008	0.08	337	5	343	426	+2
8.1	e,p,osc	392	138	0.35	18.2	1.6E-3	2.87	18.02	0.2	0.0770	0.0048	18.55	0.2121	0.05417	0.0059	0.403	0.0443	0.0539	0.0006	0.10	338	4	378	246	+11
9.1	e,p,osc	538	104	0.19	25.0	8.4E-4	1.53	18.16	0.2	0.0660	0.0033	18.45	0.1625	0.05330	0.0039	0.398	0.0293	0.0542	0.0005	0.12	340	3	341	165	+0
10.1	e,p,osc	275	65	0.24	12.5	1.9E-3	3.44	18.28	0.3	0.0810	0.0057	18.93	0.3167	0.05356	0.0072	0.390	0.0528	0.0528	0.0009	0.12	332	5	353	303	+6
11.1	e,p,osc	365	73	0.20	17.0	1.1E-3	2.09	18.04	0.2	0.0710	0.0044	18.42	0.1709	0.05394	0.0051	0.404	0.0383	0.0543	0.0005	0.10	341	3	368	213	+8
12.1	e,p,osc	670	117	0.17	30.8	5.0E-4	0.92	18.52	0.2	0.0600	0.0006	18.69	0.1967	0.05280	0.0022	0.390	0.0169	0.0535	0.0006	0.24	336	3	320	96	-5
Sample TAB-40																									
3.1	e,fr,osc	744	208	0.28	28.8	8.70E-04	1.59	21.82	0.2	0.066	0.003	22.17	0.2	0.05327	0.0045	0.331	0.0284	0.0451	0.0004	0.11	284	3	340	193	-5
7.1	m,fr,hd	129	107	0.83	4.9	5.50E-03	10.08	20.27	0.5	0.133	0.0198	22.54	0.67	0.05167	0.0256	0.316	0.1566	0.0444	0.0013	0.06	280	8	271	1134	+10
8.1	e,p,hb	314	131	0.42	12	2.90E-03	5.21	21.29	0.2	0.094	0.0101	22.46	0.3	0.05171	0.0122	0.317	0.075	0.0445	0.0006	0.06	281	4	273	540	+1
12.1	e,r,hb	194	103	0.53	7.7	7.00E-03	12.76	18.97	0.4	0.155	0.0167	21.75	0.61	0.05243	0.0228	0.332	0.1446	0.046	0.0013	0.06	290	8	304	989	+5
1.1	e,fr,osc	323	160	0.49	14.8	1.60E-03	2.88	18.26	0.2	0.077	0.0048	18.8	0.23	0.05375	0.006	0.394	0.0443	0.0532	0.0006	0.11	334	4	361	252	+7
2.1	e,p,osc	564	85	0.15	26.1	7.70E-04	1.4	18.3	0.2	0.064	0.0034	18.56	0.16	0.05284	0.0038	0.392	0.0287	0.0539	0.0005	0.12	338	3	322	165	+14
4.1	e,fr,sc	413	178	0.43	19.8	4.90E-03	8.84	16.33	0.2	0.125	0.0085	17.92	0.33	0.05417	0.0158	0.417	0.1216	0.0558	0.001	0.06	350	6	378	655	-1
5.1	e,fr,osc	451	179	0.4	20.9	1.60E-03	2.86	18.01	0.2	0.076	0.0038	18.54	0.18	0.05319	0.005	0.396	0.0374	0.0539	0.0005	0.1	339	3	337	213	0
6.1	m,fr,osc	164	73	0.44	7.3	3.50E-03	6.36	18.08	0.3	0.104	0.0118	19.3	0.33	0.05316	0.0149	0.38	0.1069	0.0518	0.0009	0.06	326	6	336	637	+8
9.1	e,p,osc	258	123	0.48	11.7	2.60E-03	4.81	17.96	0.2	0.092	0.0101	18.86	0.24	0.05349	0.0123	0.391	0.0901	0.053	0.0007	0.06	333	4	350	520	+7
10.1	m,p,osc	205	92	0.45	9.5	3.50E-03	6.34	17.38	0.3	0.105	0.0132	18.56	0.36	0.05385	0.0159	0.4	0.1187	0.0539	0.001	0.07	338	6	365	667	+5
11.1	e,fr,osc	751	72	0.1	34.5	1.40E-03	2.54	18.23	0.3	0.074	0.0046	18.71	0.3	0.05318	0.0054	0.392	0.0405	0.0535	0.0009	0.16	336	5	336	231	-1

Error in Temora reference zircon calibration was 0.36% for the analytical session

* Common Pb corrected using measured ^{204}Pb.

Errors are 1-sigma; 206Pbc and f206 % indicate the common and radiogenic portions, respectively.

Grain characteristics (GCh) and site of the spot (SS): Site of the spot: e = end or edge, m = middle. Habit of the grain: p = prism, fr = fragmented, rd = round. CL images: osc = oscillatory zoning, hb = homegeneous bright, hd = homogeneous dark, sc = sector zoning.

Table 2. *Whole-rock compositions from the Tabaquito granitoids and dykes.*

Rock type[a]	Grd	Grd	Grd	Grd	MME	Grd	FD	MD	FD
Latitude (S) Longitude (W)	28°55'43.3" 69°08'47.1"	28°56'1.1" 69°08'29"	29°06'43.9" 69°18'52"	29°08'39.3" 69°21'10.5"	29°08'39.3" 69°21'10.5"	29°07'48.2" 69°20'35.3"	29°07'6.9" 69°18'26.6"	28°55'10.7" 69°06'45.9"	28°55'9.1" 69°06'20"
Samples	TAB-11	TAB-20	TAB-24	TAB-31	TAB-32	TAB-34	TAB-23	TAB-40	TAB-41
Major Elements (wt.%)									
SiO_2	66.02	65.63	66.92	66.04	55.04	65.05	73.88	55.84	68.35
TiO_2	0.65	0.59	0.56	0.64	0.95	0.67	0.13	0.78	0.47
Al_2O_3	15.93	15.68	15.22	14.83	15.80	15.91	13.71	18.31	15.33
FeO	4.28	3.83	3.67	4.46	7.66	4.09	1.15	7.11	2.91
MnO	0.07	0.06	0.06	0.08	0.21	0.06	0.02	0.15	0.05
MgO	1.70	1.69	1.59	2.26	6.04	2.05	0.07	3.49	1.21
CaO	3.77	3.66	3.14	2.17	5.26	3.28	0.24	5.06	2.35
Na_2O	3.15	3.05	2.92	3.05	3.30	3.01	2.98	3.76	3.88
K_2O	3.27	3.64	3.79	4.32	3.08	3.79	5.84	2.23	2.97
P_2O_5	0.17	0.15	0.15	0.17	0.19	0.17	0.09	0.31	0.13
LOI	0.80	1.40	1.30	1.20	1.30	1.20	0.72	2.97	1.83
TOTAL	99.81	99.38	99.32	99.22	98.83	99.28	98.83	100.01	99.48
X_{Fe}	0.72	0.69	0.70	0.66	0.56	0.67	0.94	0.67	0.71
MALI	2.65	3.03	3.57	5.20	1.12	3.52	8.58	0.93	4.50
ASI	1.02	1.00	1.04	1.09	0.86	1.06	1.18	1.03	1.11
Trace elements (ppm)									
Cs	5.8	4.7	6.8	9.8	8.4	13.3	10.1	2.9	3.1
Rb	124	154	157	191	162	168	336.7	82.7	94.5
Sr	361	332	233	290	230	330	44.8	587	359.2
Ba	704	629	464	616	353	593	315	1048	630
La	36	38.6	30.5	32.0	25.0	33.2	21.2	21.8	25.2
Ce	73.9	75.1	60.3	65.1	66.1	64.8	54.3	49.2	46.4
Pr	8.5	8.4	7.0	7.4	9.1	7.2	5.85	5.67	5.07
Nd	31	31.2	27.4	27.4	40	30.2	20.1	22.4	16.9
Sm	6.38	5.77	5.34	5.12	8.09	5.43	4.84	4.78	3.03
Eu	1.51	1.25	1.07	1.09	1.71	1.13	0.31	1.3	0.83
Gd	5.36	5.38	5.14	4.68	7.23	4.84	4.49	4.03	2.6
Tb	0.87	0.85	0.77	0.72	1.19	0.72	0.7	0.55	0.33
Dy	5.21	4.68	4.63	4.04	7.02	4.16	3.74	3.18	1.93
Ho	1.04	0.99	1.02	0.83	1.41	0.81	0.82	0.73	0.41
Er	2.82	2.98	2.92	2.44	4.29	2.40	2.21	2.01	1.09
Tm	0.41	0.41	0.42	0.35	0.63	0.36	0.35	0.32	0.15
Yb	2.61	2.74	3.06	2.36	4.18	2.38	2.17	1.93	0.96
Lu	0.40	0.45	0.47	0.37	0.62	0.34	0.34	0.33	0.18
U	2.68	2.40	2.60	3.60	2.50	1.50	3.7	1.3	2.5
Th	14.30	14.20	13.70	14.50	4.20	12.80	18.5	5.3	8
Y	26.9	26.0	24.3	22.3	39.4	22.3	20.4	19.3	11
Nb	11.6	11.7	10.2	11.3	12.0	11.0	8.8	8.7	9.5
Zr	191	187	385	159	135	155	78.2	119	145
Hf	5.2	5.3	9.6	4.3	3.9	4.4	3.3	3.5	4.2
Ta	1.06	0.90	1.10	1	1.10	1	1.8	0.7	1
Sc		11	12	12	21	11	5	13	5
V		88	79	96	161	98	18	121	53
Ga	20	19.7	16.4	17.1	19.6	17.4	15.4	19.4	17.4
Pb	19.1						4.2	15.7	15.4
$(La/Lu)_N$	9.34	8.9	6.74	8.98	4.19	10.1	6.47	6.86	14.5
Nb/Ta	10.9	13	9.27	11.3	10.9	11	4.89	12.43	9.5
$(Th/Ta)_N$	6.28	7.34	5.8	6.75	1.78	5.96	4.78	3.52	3.72
Eu/Eu*	0.79	0.68	0.62	0.68	0.68	0.67	0.2	0.9	0.9
Isotopes									
$^{87}Rb/^{86}Sr$	0.994		1.956		2.037				
$^{87}Sr/^{86}Sr$	0.709832		0.715012		0.715022				
error $^{87}Sr/^{86}Sr$ (2s%)	0.000003		0.000005		0.000004				
$^{87}Sr/^{86}Sr_i$	0.705277		0.70563		0.70525				
$^{147}Sm/^{144}Nd$	0.124		0.118		0.122				
$^{143}Nd/^{144}Nd$	0.512403		0.512342		0.512381				
error $^{143}Nd/^{144}Nd$ (2s%)	0.000002		0.000001		0.000001				
$^{143}Nd/^{144}Nd_i$	0.512141		0.512082		0.512111				
εNd_i	-1.61		-2.38		-1.81				
T_{DM}	1091		1113		1102				

[a] FD, felsic dike; Grd, granodiorite; MF, mafic dike; MME, mafic microgranular enclave.

Table 3. *Summary of P–T conditions in mineral assemblages from the Tabaquito granitoids.*

Sample		TAB-11	TAB-34	TAB-34	TAB-32	TAB-32	TAB-32
Rock type		granodiorite	granodiorite	granodiorite	enclave	enclave	enclave
Description		aggregates	aggregates	single crystals	included in Plg*	matrix	aggregates
Geothermometers (ºC)	Calibration uncertity						
		n = 5	n = 7	n = 3	n = 10	n = 2	n = 9
Ridolfi et al. (2010) - Eq.1	± 35 ºC	751 ± 9 (738-760)	747 ± 12 (728-769)	779 ± 17 (762-796)	754 ± 29 (720-810)	743 ± 16 (731-754)	732 ± 13 (709-742)
		n = 5	n = 7	n = 3	n = 10	n = 2	n = 9
Ridolfi & Renzulli (2012) - Eq.2	± 32 ºC	763 ± 15 (745-785)	754 ± 13 (737-770)	784 ± 29 (752-810)	748 ± 33 (722-804)	752 ± 5 (749-756)	748 ± 20 (716-786)
		n = 5	n = 7	n = 3	n = 10	n = 2	n = 9
Putrka (2016) - Eq.5	± 30 ºC	733 ± 15 (722-743)	726 ± 8 (720-740)	755 ± 20 (738-777)	741 ± 22 (716-781)	732 ± 0	724 ± 11 (705-736)
Holland & Blundy (1994)	± 40 ºC	n = 20	n = 25	n = 21	n = 14	n = 16	n = 32
		An (%mol): 42-49	An (%mol): 42-46	An (%mol): 34-46	An (%mol): 41-48	An (%mol): 21-46	An (%mol): 42-48
Ed–Q–Tr–Ab thermometer (P = 2 kbar)		-	-	754 ± 30 (708-801)	762 ± 14 (740-782)	641 ± 27 (604-689)	-
Ed–Ab–Rich–An thermometer (P = 2 kbar)		800 ± 15 (777-825)	746 ± 15 (720-775)	767 ± 20 (726-795)	756 ± 10 (739-769)	666 ± 32 (623-725)	742 ± 15 (717-782)
Geobarometers (kbar)	Calibration uncertity						
		n = 5	n = 7	n = 3	n = 10	n = 2	n = 9
Schmidt (1992)	± 0.6 kbar	1.8 ± 0.2 (1.5-1.9)	2.0 ± 0.4 (1.4-2.5)	2.8 ± 0.4 (2.4-3.1)	1.9 ± 0.8 (1.0-3.6)	1.7 ± 0.6 (1.3-2.1)	1.4 ± 0.4 (0.8-1.9)
Mutch et al. (2016)	± 0.5 kbar	1.9 ± 0.1 (1.7-1.9)	1.9 ± 0.2 (1.6-2.2)	2.4 ± 0.2 (2.4-2.6)	1.9 ± 0.4 (1.5-2.9)	1.8 ± 0.3 (1.6-2.0)	1.7 ± 0.2 (1.4-1.9)
				n = 19 (T = 750 ºC)	n = 13 (T = 750 ºC)	n = 9 (T = 650 ºC)	
				An (%mol): 34-46	An (%mol): 41-48	An (%mol): 21-46	
Molina et al. (2015)	± 1.5 to ± 2.3 kbar	-	-	1.7 ± 0.6 (0.7-2.6)	2.2 ± 1.1 (0.7-3.7)	1.9 ± 0.7 (0.8-3.3)	-

*Abbreviations: Plg, plagioclase.